Earth and Planetary Science Letters 619 (2023) 118283

Contents lists available at ScienceDirect

Earth and Planetary Science Letters

journal homepage: www.elsevier.com/locate/epsl

An innovative isotopic method to identify the volcanic source of distal tephra

Mathilde Bablon [a,*], François Nauret [b], Marianne Saillard [a], Pablo Samaniego [b], Ivan Vlastélic [c], Silvana Hidalgo [d], Jean-Luc Le Pennec [e], Gueorgui Ratzov [a], François Michaud [f], Patricia Mothes [d], Céline Liorzou [e], Abdelmouhcine Gannoun [b]

[a] Université Côte d'Azur, CNRS, IRD, Observatoire de la Côte d'Azur, Géoazur, Valbonne, France
[b] Laboratoire Magmas et Volcans, Université Clermont Auvergne, CNRS, IRD, OPGC, Clermont-Ferrand, France
[c] Observatoire volcanologique et sismologique de la Guadeloupe IPGP, Le Houelmont, 97113 Gourbeyre, Guadeloupe
[d] Instituto Geofísico, Escuela Politécnica Nacional, Ap. 17-01-2759, Quito, Ecuador
[e] IRD, Geo-Ocean, Univ Brest, CNRS, Ifremer, UMR6538, Institut Universitaire Européen de la Mer, 29280 Plouzané, France
[f] Université Côte d'Azur, Sorbonne Universités, CNRS, Observatoire de la Côte d'Azur, IRD, Géoazur, France

ARTICLE INFO

Article history:
Received 13 January 2023
Received in revised form 19 June 2023
Accepted 20 June 2023
Available online 26 July 2023
Editor: C.M. Petrone

Keywords:
tephrochronology
distal tephra correlation
Pb isotope ratios
Andean arc

ABSTRACT

Identifying the sources of distal tephra in marine sediments or polar ice provides clues on the dynamic and large-scale impact of major volcanic eruptions. However, determination of the volcanic source of distal tephra is challenging due to size-dependent fractionation during atmospheric transport that modifies the mineral, chemical and even isotope composition of the transported and settled tephra. The composition of distal fine ash may thus be different from the coarser proximal products of the same eruption. Identifying the volcanic source of distal ash using the compositional data may therefore prove difficult. To get around this modification of distal composition, we propose here a new isotopic method to identify the source of distal tephra that is not based on raw transport-dependent isotope ratios but on two-dimension Pb isotope mixing lines, which account for atmospheric fractionation processes. To demonstrate the robustness of our method, we used the extensive database of Pb isotope compositions of volcanic products from the Northern Andean arc, to which we append 68 new Pb isotopic analyses obtained on proximal and distal eruptive tephra. We show for the first time that proximal products define a straight line in the $^{208}Pb/^{206}Pb$-$^{207}Pb/^{206}Pb$ space, whose equation is specific to each volcanic source. We then show that distal co-genetic tephra plot on the same line as proximal products, implying that the isotopic lines are robust fingerprints of volcanic sources that do not depend on the age, mineral assemblage, and nature of the emitted products. This new method uses bulk rock analyses and therefore provides a new perspective on distal tephra correlation and source identification in the Andes and probably other volcanic arcs with significant Pb isotopic variations.

1. Introduction

During explosive volcanic eruptions, gas and pyroclastic particles (tephra; i.e., bombs, lapilli and ash, composed of volcanic glass and minerals) are emitted into the atmosphere. Finest pyroclastic particles can be transported over tens, hundreds or even thousands of kilometers of distance depending on the size and dynamics of the eruption, and atmospheric effects (i.e., Lowe, 2011; Brown et al., 2012). Coupled with the determination of their age, the identification of the volcanic source of distal tephra fall deposits and their correlation with proximal well-studied eruptive products help for reconstructing paleoenvironments (e.g., Newnham et al., 1998; Siani et al., 2013; Wulf et al., 2018), the eruptive history of a region (e.g., Caron et al., 2012; Schindlbeck et al., 2016), studying human settlements in archaeology (e.g., Guillaume-Gentil, 2008), and the evolution of past global climate (e.g., Costa et al., 2012; Timms et al., 2018; Nomade et al., 2019). In addition, the study of distal tephra is sometimes the only way to trace the eruptive history of a volcanic system when proximal deposits are eroded or concealed below younger ones (Bourne et al., 2010; Schindlbeck et al., 2015).

The identification of the volcanic source of distal tephra layers is based on the characterization of the tephra and its comparison to proximal deposits of eruptive centers. Multiple independent

* Corresponding author.
E-mail address: mathilde.bablon@geoazur.unice.fr (M. Bablon).

https://doi.org/10.1016/j.epsl.2023.118283

datasets are necessary to establish strong correlations. The chronological constraints (e.g., absolute dating, stratigraphic position, archaeological remains), the mineralogical assemblage of tephra layers, the morphology of glass shards, and the major-trace geochemistry of volcanic products are commonly used (e.g., Lowe, 2011). However, identifying the volcanic source of distal tephra is tricky because atmospheric transport generates grain size sorting that can result in mineralogical fractionations (Carey and Sigurdsson, 1982). The mineral assemblage and the bulk geochemical compositions of distal products may therefore be significantly different from those of proximal products (e.g., Sarna-Wojcicki and Davis, 1991; Bablon et al., 2022). It is accordingly necessary to develop a method for the identification of the source of distal tephra that does not depend on either mineralogical composition or the absolute value of a reference geochemical composition given by the proximal products.

Recent tephrochronological works have used single-grain approach calling on LA-ICP-MS techniques (e.g., Schindlbeck et al., 2016; D'Antonio et al., 2016; Wulf et al., 2018). Such approach allows to detect heterogeneities of chemical composition (i.e., major and trace element contents, and isotope ratios), to perform measurements on fine glass shards (10–20 µm; e.g., Ukstins Peate et al., 2003; Westgate et al., 2011), to analyze very small volumes of tephra present in deep sea or ice cores, and to avoid issues related to mechanical fractionation. However, single-grain data of proximal products are not always available for comparison with distal tephra.

In this paper, we propose a new and complementary method for identifying the volcanic source of distal tephra based on the isotopic composition of Pb, using a bulk analysis approach. The method is tested on selected tephra deposits from the Northern Andes, where the resolution of tephrochronological methods has strong limitations because of the high number of volcanoes and eruptions. For this purpose, we take advantage of the well-studied Ecuadorian arc, for which many previous studies have identified the largest Holocene eruptions of this arc segment (e.g., Hall and Mothes, 2008a), which produced distal tephra layers that are found in the coastal plain (onshore) and offshore (Bablon et al., 2022). Few geochemical analyses have been performed on single-grain for proximal products in this region. The new correlation method proposed in this paper therefore presents the advantage of being applicable in study areas where geochemical analyses are predominantly performed on whole-rock samples of lava flows or juvenile blocks of Pyroclastic Density Currents (PDC). Moreover, our new method is an additional correlation tool in regions where products from different volcanic sources have similar major and trace element contents, and therefore where the identification of the volcanic source of the distal tephra by comparison of their geochemical composition is difficult.

2. Geological context

The volcanism of the Northern Volcanic Zone (NVZ) of the Andes (5°N to 2°S) originates from the subduction of the oceanic Nazca plate beneath the continental South American plate (Fig. 1). With more than 76 volcanic centers of Quaternary age (Hall et al., 2008), Ecuador is hosting the major part of that volcanism. Among these volcanoes, at least eight experienced Plinian eruptions during the Holocene. Extensive volcanological studies carried out over the past 20 years have documented the eruptive history of numerous eruptive centers such as Cotopaxi (e.g., Hall and Mothes, 2008b; Garrison et al., 2011), Pichincha (e.g., Robin et al., 2010; Samaniego et al., 2010), Tungurahua (e.g., Hall et al., 1999; Le Pennec et al., 2016), Cayambe (e.g., Samaniego et al., 2010), and Atacazo-Ninahuilca (Hidalgo, 2006; Hidalgo et al., 2008), as well as at the whole arc scale (e.g., Barberi et al., 1988; Hidalgo et al., 2012; Ancellin et al., 2017; Bablon et al., 2019, 2020; Chiaradia et al., 2021), resulting in a large geochemical and geochronological dataset. With the exception of rhyolitic calderas that were active since more than 2.5 Ma (Opdyke et al., 2006), ages obtained on oldest deposits of the present arc range from 1.3 to 1.0 Ma (Samaniego et al., 2010; Hidalgo, 2006; Robin et al., 2010; Bablon et al., 2020). The volcanic activity has intensified over the last 500–300 kyr, and about 24 volcanoes were active during the Holocene (e.g., Hall et al., 2008). Magmas of eruptive centers located in the Andean Cordillera mainly display medium-to-high K calc-alkaline andesite and dacite compositions, and contrast with alkaline basalts and basaltic andesites of the easternmost volcanoes of the Sub-Andean zone (e.g., Hidalgo et al., 2012; Ancellin et al., 2017). During explosive eruptions, lapilli and ash fall on the flanks of volcanoes and on the surrounding areas, whereas smallest particles (fine to very fine ash) are mostly transported towards the coastal region by atmospheric currents, and can reach the Pacific Ocean (e.g., Vallejo Vargas, 2011; Jackson et al., 2019; Bablon et al., 2022).

In this study, we mainly focus on tephra of well-documented major explosive eruptions of Holocene age, whose deposits are exposed and easily recognizable in the Cordillera and the coastal area. A brief description of these main Plinian eruptions is given below.

The eruptive history of ***Atacazo-Ninahuilca*** volcanic complex, located 10 km southwest of Quito (Fig. 1e), started about 1.29 Ma ago (Hidalgo, 2006). It experienced at least four periods of explosive activity (called "N3" to "N6") during the Holocene, recorded by thick deposits of tephra fall and PDC (Hidalgo et al., 2008). Radiocarbon ages indicate that these events occurred at ~ 9950, ~ 6200, ~ 4950 and ~ 2300 cal BP, respectively (Hidalgo et al., 2008). Tephra layers of the N2, N4 and N5 events have been identified in the coastal area and in marine sediments (Vallejo Vargas, 2011; Bablon et al., 2022).

The largest eruption of ***Chachimbiro*** volcano, located north of Cotacachi (Fig. 1c), occurred between 5590 and 5460 cal BP and produced a large PDC deposit that crops out abundantly on the eastern side of the volcanic complex (Bernard et al., 2014).

Cotopaxi volcano (Fig. 1b) experienced five major rhyolitic episodes between ~ 13 and ~ 5 ka (called "F series"; Hall and Mothes, 2008b). The largest eruptions occurred 7160–8600 and 6550–6800 cal BP (F2 and F4 events, respectively), associated with the deposition of about 5–8 km^3 of tephra until the Pacific margin (Hall and Mothes, 2008b; Bablon et al., 2022). This sequence is covered by the Colorado Canyon rhyolite episode that occurred between 5320 and 4530 cal BP (Hall and Mothes, 2008b; Bablon et al., 2022). It led to a large PDC deposit that crops out on the northern flank of the volcano. Furthermore, its composition differs from other products of Cotopaxi, with a geochemical signature similar to that of Chalupas caldera, located southeast of Cotopaxi (Garrison et al., 2011; Bablon et al., 2022).

Cuicocha caldera, located 50 km north of Quito (Fig. 1c), presently filled by a lake, was formed during a large explosive eruption that took place after a dome destruction between 3695 and 3060 cal BP, based on radiocarbon ages obtained on organic material from the associated PDC deposits (Hall and Mothes, 1994; Almeida et al., 2023). A tephra layer identified in marine terraces has been linked to this eruption (Vallejo Vargas, 2011).

North of Atacazo, ***Pichincha*** volcanic complex (Fig. 1d) experienced four main eruptive phases with major Plinian eruptions during the last 3 ka (Robin et al., 2008). Radiocarbon ages performed on charcoal debris present in soil between resulting tephra fall and PDC deposits indicate that those explosive events occurred at ~ 3200, ~ 1900, ~ 1000 and ~ 400 cal BP (Robin et al., 2008). Tephra layers of the 10th century and the ~ 3200 cal BP eruptions

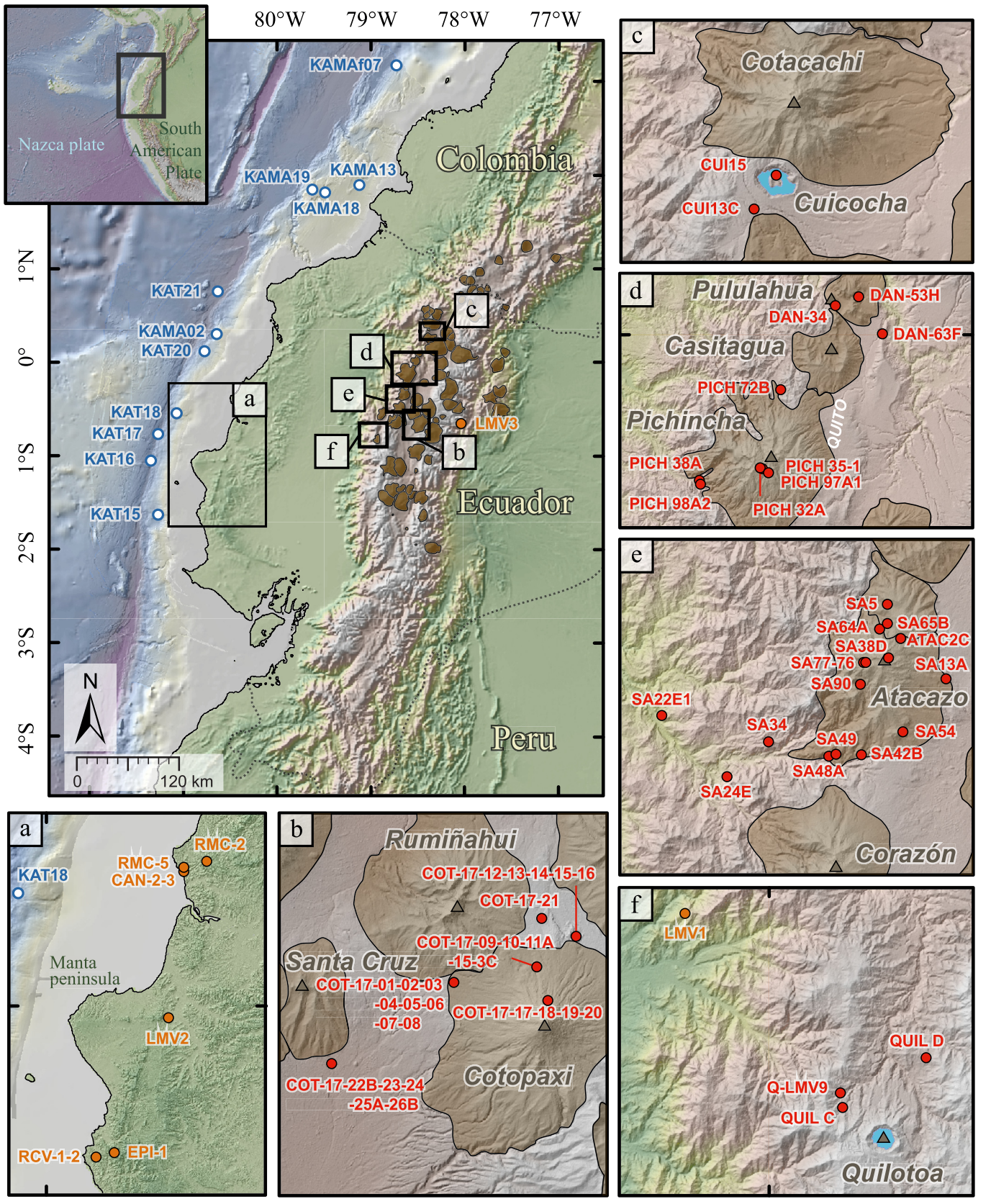

Fig. 1. Geological context of the Ecuadorian volcanic arc. Quaternary volcanoes are represented in brown (Bernard and Andrade, 2011). Locations of marine coring sites mentioned in this study are represented with blue and white dots. Insets: locations of onland proximal and distal samples analyzed in this study are represented with red and orange dots, respectively, with shaded relief views of 30-m resolution SRTM Digital Elevation Models. Geographic coordinates of all samples are given in Appendix A and G.

have been identified in the coastal plain and in marine sediments (Vallejo Vargas, 2011; Bablon et al., 2022).

North of Pichincha, ***Pululahua*** (Fig. 1d) experienced at least four explosive eruptive events between 2595–2495 and 2350–2335 cal BP, leaving thick succession of pumice-rich tephra fall and PDC deposits (Papale and Rosi, 1993; Andrade et al., 2021).

The crystal-rich deposits of the most recent eruption of ***Quilotoa*** volcano (Fig. 1f), which occurred 730–680 cal BP, constitute a stratigraphic marker over almost the entire Ecuadorian arc covering an area of $\sim 810\,000$ km^2 and exposed in the coastal region (Rosi et al., 2004; Mothes and Hall, 2008; Di Muro et al., 2008; Vallejo Vargas, 2011; Bablon et al., 2022).

The major and trace elements compositional fields of the products of these different eruptions partially overlap (Bablon et al., 2022), making the identification of the volcanic source of distal tephra uncertain. This identification is also complicated by the fact that several major eruptions are coeval. Such situation occurred especially between 4800 and 5000 cal BP for the Colorado Canyon and Atacazo-Ninahuilca N5 events considering age uncertainties at the 1-σ level (Bablon et al., 2022), but the trace elements of these eruptions allow us to distinguish between them, since their source is located in the Eastern and Western Cordillera, respectively.

3. Pb isotope geochemistry

In volcanic arcs, the variation in the Pb isotopic compositions reflects the mixing between the mantle wedge component, and other components derived from the subducted slab and/or the arc crust (DePaolo, 1981; Arculus and Powell, 1986; Ishikawa and Nakamura, 1994). In a 3-D $^{206}Pb/^{204}Pb$-$^{207}Pb/^{204}Pb$-$^{208}Pb/^{204}Pb$ space, these ternary mixtures are represented by planes whose geometry depends on the isotope composition of the end-members involved in the magma genesis processes. In arcs constructed on thick continental crust, the assimilation of the continental crust is ubiquitous, and the isotopic composition of ensuing volcanic products is therefore a function of the local composition of the continental crust, and the degree of crustal assimilation (e.g., Mamani et al., 2008; Ancellin et al., 2019; and many others). The isotope signature of these volcanic rocks highly depends on their mineral assemblage. Indeed, minerals formed during the crystallization sequence along the magmatic column are not in isotopic equilibrium (Davidson et al., 2001, 2007; Ancellin et al., 2019). For instance, amphibole crystals in Guagua Pichincha dacites present higher $^{207}Pb/^{206}Pb$ and $^{208}Pb/^{206}Pb$ ratios than plagioclase crystals of the same magma (Fig. 2a, b). The later a mineral crystallizes, the closer its isotopic composition to the assimilated continental crust (Ancellin et al., 2019). The modal mineral assemblage, and consequently the degree of differentiation, therefore governs the isotopic composition of an andesite-dacite volcanic product (Nauret et al., 2018). As a consequence, the isotopic composition of distal tephra may be different from that of proximal eruptive products collected on the flanks of a volcano, due to the mineralogical sorting that occurs during atmospheric transport of tephra. The isotopic imbalance of minerals prevents accurate identification of the volcanic source of distal tephra by direct comparison with the isotopic signature of proximal products.

4. Materials and methods

4.1. Database and sampling strategy

Sixty-nine new Pb analyses of lava flows and tephra have been performed in this study. The latter was made possible given the current knowledge of volcanic records of Ecuadorian volcanoes provided by the important work performed during the two last decades in Ecuador (Hidalgo, 2006; Hidalgo et al., 2008; Hall and Mothes, 2008b; Mothes and Hall, 2008; Robin et al., 2008, 2010; Samaniego et al., 2010; Vallejo Vargas, 2011; Andrade et al., 2021; Almeida et al., 2023). These studies allowed us to carefully select samples from the geological archives, which correspond to key volcanic stages and key explosive events that affected the Cordillera and coastal region during the Holocene. To check the reliability of our correlation method based on proximal eruptive products, we used in a second step measurements performed on distal onshore and offshore tephra beds correlated to major Holocene eruptions (Vallejo Vargas, 2011; Bablon et al., 2022), then applied our method to distal tephra of unknown sources.

Fifty-eight proximal samples were collected from six Ecuadorian eruptive centers (red dots, Fig. 1). Geographical coordinates and nature of the samples are listed in Appendix A. Twenty-seven proximal Holocene tephra were sampled in five sites in the northern and western flanks of ***Cotopaxi*** volcano (Fig. 1b). Three of them (COT-17-09, COT-17-10 and COT-15-3C) belong to the Colorado Canyon unit (4530–5320 cal BP; Hall and Mothes, 2008b; Bablon et al., 2022), five samples (COT-17-22 to COT-17-26B) belong to the F series (~ 13 to ~ 5 ka; Hall and Mothes, 2008b), one sample (COT-17-21) to the Peñas Blancas event (~ 2100 y BP; Hall and Mothes, 2008b), and two samples (COT-17-19 and COT-17-20) lie above the Quilotoa ash bed. Photographs of field and outcrops are available in Appendix B. Five pumice samples from large eruptions that occurred between the 1st century and 1660 AD were collected in the northern and southern flanks, and summit area of ***Pichincha*** volcano (Robin et al., 2008, 2010). We collected four samples of lavas and pumices from ***Pululahua*** volcano (Fig. 1d) that were emitted during the late Pleistocene (DAN-53H), the major 2.3–2.6 ka event (Andrade et al., 2021; DAN-63F and PICH 72B), and the last 2.2 ka eruption (DAN-34). We also performed new measurements of Pb isotope ratios on 17 lava flows and pumice samples previously collected as part of the study of the eruptive history of ***Atacazo-Ninahuilca volcano*** (Hidalgo, 2006), and belonging to different volcanic units (Fig. 1d; Hidalgo et al., 2008). In addition, we analyzed two pumice samples from the ***Cuicocha*** caldera (Fig. 1c), emitted during the 3695–3060 cal BP eruption, whose mineralogy and geochemistry are given in Almeida et al. (2023), as well as three pyroclastic samples from the 730–680 cal BP eruption of ***Quilotoa*** volcano (Fig. 1f), the westernmost eruptive center of Ecuador (Fig. 1).

We used measurements performed on twelve distal tephra beds present in marine cores offshore Ecuador and southern Colombia (white and blue dots, Fig. 1). Based on their mineralogy, major and trace element contents, ^{14}C ages, as well as Sr and Pb isotope ratios, they have been correlated to Holocene eruptions from the Colombian Cerro Machín and Ecuadorian Cotopaxi, Pichincha, and Atacazo-Ninahuilca volcanoes (Bablon et al., 2022). We also performed new measurements of Pb isotope ratios on tephra present in the coastal region (Fig. 1a), which have been correlated to Holocene eruptions from Cotopaxi (CAN-3 and RCV-2), Quilotoa (RMC-2) and Pichincha (RCV-1) volcanoes, based on their mineralogy and major-trace geochemistry (Vallejo Vargas, 2011). Three other distal tephra have been correlated to Cotopaxi (RMC-5), Pululahua (RMC-2) and Pichincha (EPI-1; Fig. 1a) volcanoes (Vallejo Vargas, 2011). However, the identification of their volcanic source is only inferred from stratigraphy and mineralogy. We therefore performed new Pb measurements on these samples to reassess their correlation. Finally, we applied our method on three tephra layers whose volcanic source is unknown, exposed at the foot of the Western Cordillera (LMV1; Fig. 1f), in the coastal region east of Manta peninsula (LMV2; Fig. 1a), and in the Eastern Cordillera northwest of the Chalupas caldera (LMV3; Fig. 1).

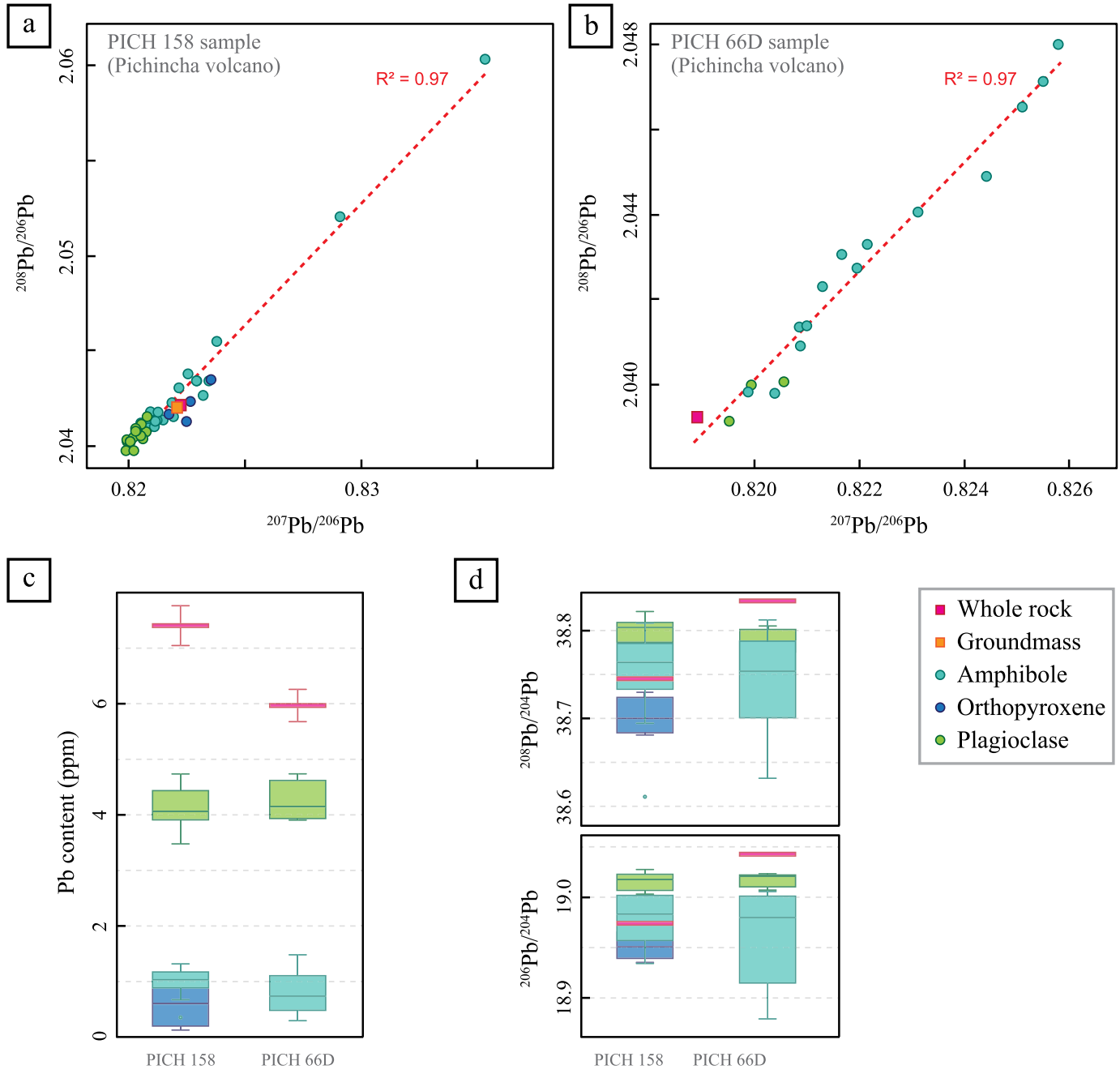

Fig. 2. Lead contents and isotope ratios of minerals, groundmass and whole rock of two proximal samples from Pichincha volcano, Ecuador (compiled Pb analyses from Ancellin et al., 2019). PICH 158 corresponds to a juvenile sample from a block-and-ash flow deposited during the 1999–2001 eruption, and PICH 66D is a juvenile block from an explosive eruption of early Holocene age (Robin et al., 2010). Both samples contain phenocrysts of plagioclase (5–20 vol.%), amphibole (5–10 vol.%), orthopyroxene (< 5 vol.%), and Fe-Ti oxides (< 2 vol.%), in a finely crystallized matrix. a–b) $^{208}Pb/^{206}Pb$ vs. $^{207}Pb/^{206}Pb$ ratios of samples PICH 158 and PICH 66D, respectively. c–d) Box plots indicating the Pb content, $^{206}Pb/^{204}Pb$ and $^{208}Pb/^{204}Pb$ ratios of components of both samples (data from Ancellin et al., 2019) The Pb content of the groundmass has not been analyzed but is expected to be higher than crystals due to the incompatible behavior of Pb. In addition, early crystallized mineral phases, such as olivine and oxide, contain less than 1 ppm of Pb because of the very low partition coefficient of Pb in these minerals.

4.2. Analytical procedure for Pb isotopic measurements

The isotopic analyses of distal tephra are generally performed by in-situ analysis (LA-ICP-MS or SIMS) on glass shards. LA-ICP-MS technique is essential to study very small tephra particles, and the accuracy of lead ratios against ^{204}Pb, better than 0.8%, is sufficient for applications in tephrochronology (e.g., Westgate et al., 2011).

We propose here an alternative and complementary method based on bulk rock analysis of distal volcanic deposits by MC-ICP-MS. The analytical procedure is detailed in Ancellin et al. (2017). About 150 mg of powdered samples were leached in a HCl solution, rinsed several times with ultrapure water, then dissolved using HNO_3, HF, and HCl solutions. After complete dissolution and evaporation, sample residues were diluted in 2 ml of 2 M HNO_3, then lead was separated using the Sr spec resin (Pin et al., 2014). This method allows the precise analysis of $^{206}Pb/^{204}Pb$, $^{207}Pb/^{204}Pb$ and $^{208}Pb/^{204}Pb$ ratios on samples containing 150 pg to 20 ng of lead (Ancellin et al., 2019), and can therefore be applied using up to ~ 1 mg of bulk tephra. However, some caution is needed for such small masses due to potential lack of sample's representativity. Pb ratios of marine tephra layers are potentially biased by contamination during sample recovery and/or by crystalliza-

tion of new minerals in vesicles or as replacement products of glass and crystals (e.g., clays, zeolite, barite, pyrite; Hanano et al., 2009). We did not observe such weathering phases in our samples (SEM images of marine tephra layers are given in the Data Set S2 of Bablon et al., 2022), which may have been preserved from prolonged interaction with seawater due to rapid burial. Regardless, HCl leaching performed during sample preparation removes any alteration microphases potentially present, and therefore removes the effects of contamination and alteration that may disturb the pristine magmatic Pb isotopic composition (Nobre Silva et al., 2009; D'Antonio et al., 2016).

Pb isotope ratios were measured on an MC-ICP-MS Neptune plus (Thermo electron) at Laboratoire Magmas et Volcans (Clermont-Ferrand, France). Instrumental mass fractionation was corrected using Tl-doping (e.g., White et al., 2000). The measured Pb ratios were normalized by linear interpolation using the $^{206}Pb/^{204}Pb$, $^{207}Pb/^{204}Pb$, and $^{208}Pb/^{204}Pb$ ratios of NBS981 standard values (16.9405, 15.4963, and 36.7219, respectively; Galer and Abouchami, 1998). We also regularly performed measurements of international standards (AGV2, RGM-1, BCR-2 and JA-1; Jochum et al., 2005), and measured twice the Pb ratios of samples LMV3 and SA34, to test the reproducibility of our results. Relative standard deviations are 50–80 ppm for $^{206}Pb/^{204}Pb$, $^{207}Pb/^{204}Pb$, and $^{208}Pb/^{204}Pb$ ratios, and < 30 ppm for the $^{208}Pb/^{206}Pb$ and $^{207}Pb/^{206}Pb$ ratios.

For proximal samples from Cotopaxi volcano, we also carried out ICP-AES measurements at the Laboratoire Geo-Ocean of the Université de Bretagne Occidentale (Brest, France) to determine their SiO_2 contents, by following the procedure detailed in Cotten et al. (1995). Results are given in Appendix C, and relative standard deviations are $\leq 1\%$.

5. Results

Lead isotope ratios measured twice on samples LMV3 and SA34 give similar results ($\Delta^{206}Pb/^{204}Pb \leq 0.004$, $\Delta^{207}Pb/^{204}Pb \leq 0.003$, and $\Delta^{208}Pb/^{204}Pb \leq 0.007$, Appendix D), and confirm the very good reproducibility of our results.

The 24 proximal samples from Cotopaxi volcano analyzed in this study are mainly andesites and rhyolites. Their SiO_2 contents range between 55.7 and 73.4 wt.%, for samples COT-17-23 and COT-17-26B, respectively (Appendix C), located west of the volcano (Fig. 1b). Lead isotope ratios vary between 18.923 and 18.980 for $^{206}Pb/^{204}Pb$ (COT-17-01 and COT-17-23, respectively), between 15.627 and 15.640 for $^{207}Pb/^{204}Pb$ (COT-17-13 and COT-17-11A, respectively), and between 38.709 and 38.765 for $^{208}Pb/^{204}Pb$ (COT-17-13 and -19, and COT-17-11A, respectively; Appendix C), in agreement with Pb values obtained elsewhere on Cotopaxi volcano (Bryant et al., 2006; Garrison et al., 2011; Ancellin et al., 2017). Hence, andesite tephra generally have the highest $^{207}Pb/^{206}Pb$ and $^{208}Pb/^{206}Pb$ ratios, whereas rhyolite tephra have the lowest $^{207}Pb/^{206}Pb$ and $^{208}Pb/^{206}Pb$ ratios.

Concerning proximal products of key Plinian eruptions of Pichincha, Atacazo-Ninahuilca, Pululahua, Cuicocha and Quilotoa volcanic centers, and of the Colorado Canyon event, $^{206}Pb/^{204}Pb$ and $^{208}Pb/^{204}Pb$ ratios range from 18.85 to 19.05, and from 38.60 to 38.85, respectively, except samples PICH 32A, ATAC 2C and QUIL C, whose ratios are significantly lower (between 18.55 and 18.70, and between 38.38 and 38.48, respectively; Appendix D). $^{207}Pb/^{204}Pb$ ratios range between 15.59 and 15.66. The most radiogenic Pb values are obtained for samples COT-17-09, COT-17-10 and COT-15-3C from Cotopaxi's Colorado Canyon unit.

Finally, $^{206}Pb/^{204}Pb$, $^{207}Pb/^{204}Pb$, and $^{208}Pb/^{204}Pb$ ratios obtained on distal tephra range between 18.93 and 19.03, 15.61 and 15.66, and 38.65 and 38.87, respectively (Appendix D). The highest values have been obtained for samples RCV-1, CAN-3 and LMV3, whereas the lowest ratios have been obtained for samples RMC-5 and CAN-2.

6. Discussion

6.1. Comparison of $^{207}Pb/^{206}Pb$ and $^{208}Pb/^{206}Pb$ ratios of proximal vs. distal volcanic products for Cotopaxi volcano

6.1.1. Analysis of Pb isotope ratios of proximal tephra from Cotopaxi volcano

Principal Component Analysis (PCA) of Pb isotope variations of proximal tephra from Cotopaxi volcano reveals that 98.72% of the isotopic variability can be described geometrically as a plane in a 3-D $^{206}Pb/^{204}Pb$-$^{207}Pb/^{204}Pb$-$^{208}Pb/^{204}Pb$ space, defined by two eigenvectors F1 and F2 (Fig. 3, Appendix E). This plane depicts the ternary mixture of components involved in the magma genesis of Cotopaxi volcano (i.e., the mantle wedge, the subducted slab, and the continental crust) already identified by various authors (e.g., Bryant et al., 2006; Garrison et al., 2011).

There is no clear correlation between $^{206}Pb/^{204}Pb$ and $^{207}Pb/^{204}Pb$ ratios, nor between $^{206}Pb/^{204}Pb$ and $^{208}Pb/^{204}Pb$ ratios (Fig. 4a). However, the plane defined in a 3-D $^{206}Pb/^{204}Pb$-$^{207}Pb/^{204}Pb$-$^{208}Pb/^{204}Pb$ space defines a straight line in a 2-D $^{207}Pb/^{206}Pb$-$^{208}Pb/^{206}Pb$ space (illustrated in Ukstins Peate et al., 2003 and Nauret et al., 2018), in which $^{207}Pb/^{206}Pb$ and $^{208}Pb/^{206}Pb$ ratios of Cotopaxi's proximal tephra display a strong positive linear correlation ($R^2 = 0.94$, Fig. 4b). Isotopic data obtained on lava flows and tephra collected on the flanks and in the vicinity of Cotopaxi volcano and carried out by TIMS (Garrison et al., 2011) are widely scattered (orange diamonds, Fig. 4a and b). This scatter is likely due to imperfect correction of instrumental Pb isotope mass bias during conventional measurements by thermal ionization mass spectrometry. As the mass fractionation is precisely corrected using Tl isotope ratios for MC-ICP-MS measurements (e.g., Belshaw et al., 1998; Rehkämper and Halliday, 1998; White et al., 2000), we use hereafter only measurements that have been carried out with this method.

Based on our new high precision data, we show that the equation of the straight line that best fits the proximal products from Cotopaxi volcano in a $^{208}Pb/^{206}Pb$ *vs.* $^{207}Pb/^{206}Pb$ diagram is $y = 2.073x + 0.334$ ($R^2 = 0.94$; Fig. 4b). This regression line does not depend on the silica content of samples (turquoise, blue and purple symbols, Fig. 4b), and therefore applies for volcanic products with different degrees of magmatic differentiation.

In arc magmas, due to the incompatible behavior of lead, the finely crystallized interstitial matrix, as well as the late crystallized minerals such as plagioclase, amphibole and biotite, dominate the Pb budget (Fig. 2c). Furthermore, minerals present heterogeneous Pb isotope ratios (Fig. 2a, b, d). However, this heterogeneity in Pb distribution, and sorting during tephra transport that results in isotopic fractionation, do not impact the reliability of our model. Indeed, the composition of a sample analyzed using a whole rock or bulk measurement belongs to the mixing line of its volcanic source (Figs. 2a, b, 4b). As a consequence, this method is particularly suitable for altered samples, as their composition will simply move along the mixing line of their volcanic source, after removing from the analyzed fraction the mineral phases, groundmass or glass shards presenting traces of weathering or alteration. However, we stress the importance of analyzing all the mineral and glass components of fresh lavas and tephra layers, in particular the early crystallized phases and volcanic products of various degrees of magmatic differentiation, to better define the mixing line.

6.1.2. Distal tephra correlated to major eruptions of Cotopaxi volcano

Three tephra layers identified in cores KAT16 and KAT17 collected offshore Ecuador (Fig. 1) have been correlated to Holocene

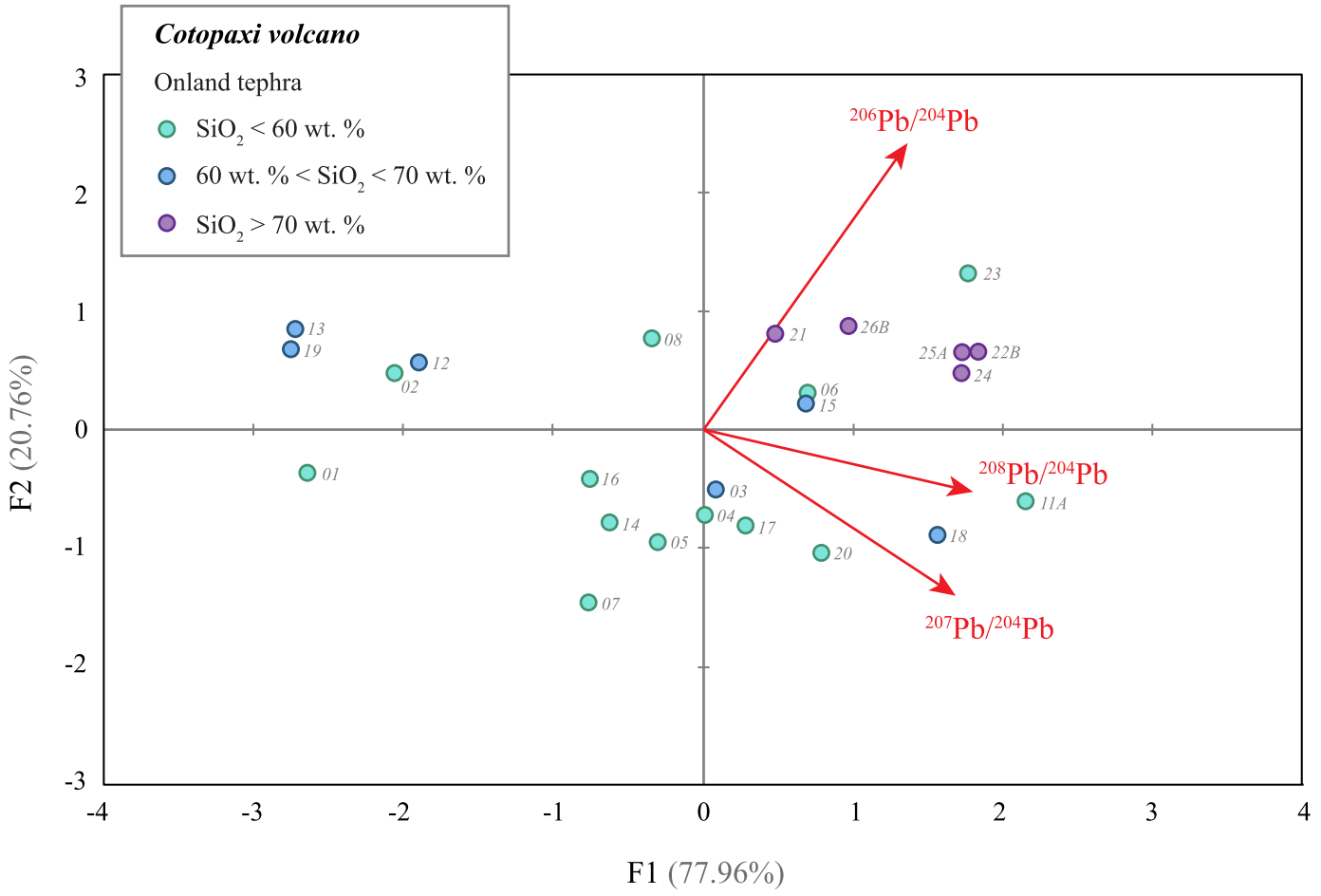

Fig. 3. Biplot diagram resulting from a Principal Component Analysis of Pb isotope variability for Cotopaxi's proximal products (Appendix C). 98.72% of the Pb isotope variability is explained by two eigenvectors, F1 encompassing 77.96% of the variability, and F2 20.76%. These two eigenvectors F1 and F2 define a plane in a 3-D $^{206}Pb/^{204}Pb$-$^{207}Pb/^{204}Pb$-$^{208}Pb/^{204}Pb$ space interpreted as reflecting mixing and assimilation processes. Gray numbers refer to sample names (COT-17-xx). 3-D animation of this figure is available in Appendix E.

eruptions of Cotopaxi volcano (Bablon et al., 2022). The $^{208}Pb/^{206}Pb$ and $^{207}Pb/^{206}Pb$ ratios measured on glass shards of these distal tephra have been reported in the scatter plot of proximal products emitted by Cotopaxi volcano (pink stars, Fig. 4). They plot on the Cotopaxi's regression line, very close to the Pb isotope composition of rhyolite samples (purple symbols, Fig. 4). The use of Pb isotope compositions, and in particular the coupling between $^{207}Pb/^{206}Pb$ and $^{208}Pb/^{206}Pb$ ratios, is therefore a powerful tool for identifying or checking the source of volcanic material, especially for distal deposits.

6.2. Database at the scale of the Northern Andean arc

Following the same approach as for Cotopaxi volcano, we have compiled published Pb isotopic data for the Northern Andean volcanic arc (Georoc database; $n = 283$; Appendix F), appended by our 54 new Pb isotope measurements carried out on proximal products (Fig. 1; Appendix C and D). $^{207}Pb/^{206}Pb$ and $^{208}Pb/^{206}Pb$ ratios are reported in Fig. 5, and regression lines of each volcanic center, for which more than two Pb analyses are available, have been represented with different colors. Equations of all regression lines are given in Table 1. The regression line of some volcanoes, such as Cerro Machín, Iliniza, Puñalica, Reventador and Sangay, have been determined based on only 3 analyses, whereas the regression line is much more representative for Yanaurcu, Chachimbiro and Tungurahua volcanoes, for which more than 40 Pb measurements are available. Coefficients of determination (R^2) are generally higher than 0.90, except for Imbabura (0.87), Pululahua (0.83), Nevado de Santa Isabel in central Colombian Andes (0.63), and Pulumbura (0.38) that should be considered with caution since authors indicate surprisingly old unpublished ages (12–13 Ma; Chiaradia et al., 2021) and analyses may correspond to the heterogeneous Miocene basement. Even though, the $^{207}Pb/^{206}Pb$ *vs.* $^{208}Pb/^{206}Pb$ diagram (Fig. 5) illustrates that the regression lines of each eruptive center are characterized by a specific slope and y-intercept. The isotope trends are not geographically related to the main volcanic sectors (i.e., Western or Eastern Cordillera, Interandean Valley or Sub-Andean zone of Ecuador, and Central Cordillera of Colombia). In addition, the equation of the regression lines appears unrelated to the age of the samples. For instance, $^{207}Pb/^{206}Pb$ and $^{208}Pb/^{206}Pb$ ratios are strongly correlated for Atacazo-Ninahuilca volcano ($R^2 = 0.97$, Table 1), whose products range in age from 1.29 ± 0.01 Ma ($^{40}Ar/^{39}Ar$ age of the oldest La Carcacha edifice; Hidalgo, 2006) to ~ 370–410 cal BC (^{14}C age of a carbonized wood in a PDC from the N6 eruptive event; Hidalgo et al., 2008). In addition, although the ages of some eruptions are very close (~ 2.2 ka for Atacazo N6 and Pululahua events, and ~ 4.9 ka for Colorado Canyon and Atacazo N5 events, for instance), we discard the possibility that ash mixtures could have introduced noise, as the mineral assemblage and the location of proximal products allow to reliably discriminate their sources. Finally, the statistical dispersion of analyses may be explained by sampling concerns, analytical errors, and possibly local heterogeneities related to deep processes (i.e., differentiation, convective mechanical phenomena,

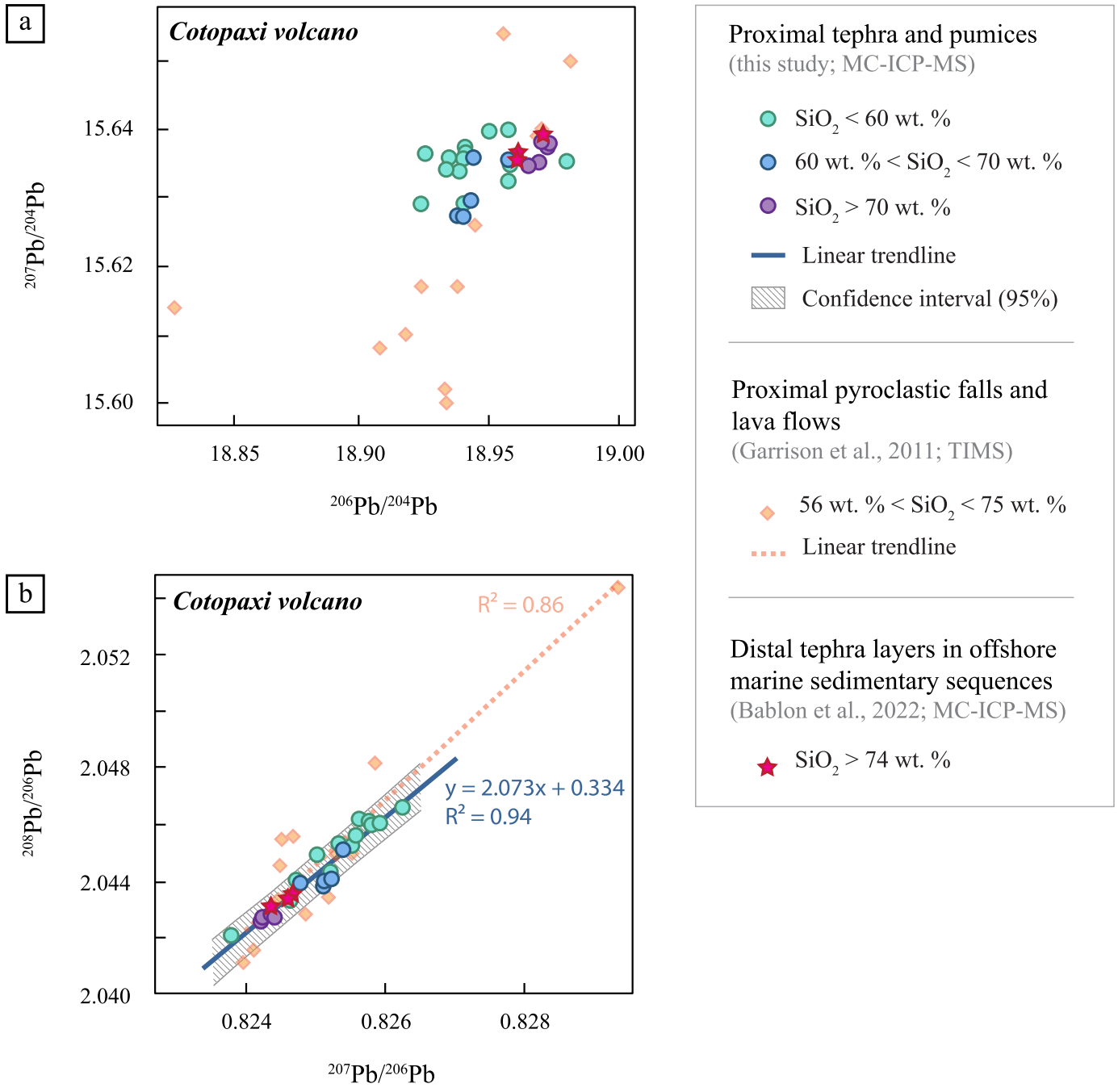

Fig. 4. Scatter plot of Pb isotope ratios of proximal products from Cotopaxi volcano. a) $^{207}Pb/^{204}Pb$ vs. $^{206}Pb/^{204}Pb$ diagram. b) $^{208}Pb/^{206}Pb$ vs. $^{207}Pb/^{206}Pb$ diagram showing a strong correlation between Pb ratios for measurements carried out using MultiCollector Inductively Coupled Plasma Mass Spectrometry (MC-ICP-MS). Ratios carried out on tephra and pumices in this study (Fig. 1b) are represented with the same colors as Fig. 3. Error bars are included in the size of the symbols. Data from the literature are represented by orange diamonds for proximal lava flows and pyroclastic fall deposits (Garrison et al., 2011), and pink stars for distal marine tephra beds (Bablon et al., 2022).

mixing) or related to the crust assimilation during the magma ascent. However, high coefficients of determination (Table 1) indicate that these processes play a minor role, and do not challenge the correlations and method.

6.3. Method validation and application to distal tephra of uncertain and unknown volcanic source

6.3.1. Method validation using distal tephra of known volcanic source

To verify that regression lines can be used to identify the volcanic source of distal deposits, we reported $^{207}Pb/^{206}Pb$ and $^{208}Pb/^{206}Pb$ ratios obtained for distal tephra whose volcanic source has been previously determined (Vallejo Vargas, 2011; Bablon et al., 2022) on correlation lines of Holocene explosive volcanoes (red stars, Fig. 6). Marine tephra ***ATAC-45***, ***-46*** and ***-49*** from cores KAT16 and 17 (Fig. 1), as well as onshore coastal tephra ***CAN-3*** and ***RCV-2*** (Fig. 1a), correlated to Cotopaxi, clearly plot on the correlation line of this volcano (red line, Fig. 6c). Their Pb ratios significantly differ from samples ***AMAD-21***, ***-34***, ***-42*** and ***ATAC-57*** (cores KAMA18, 19, 13 and KAT20, respectively; Fig. 1). These latter align well with the correlation line of Colorado Canyon's magma (including products from the Chalupas caldera and Colorado Canyon event, pink line, Fig. 6c), to which they were previously correlated (Garrison et al., 2011).

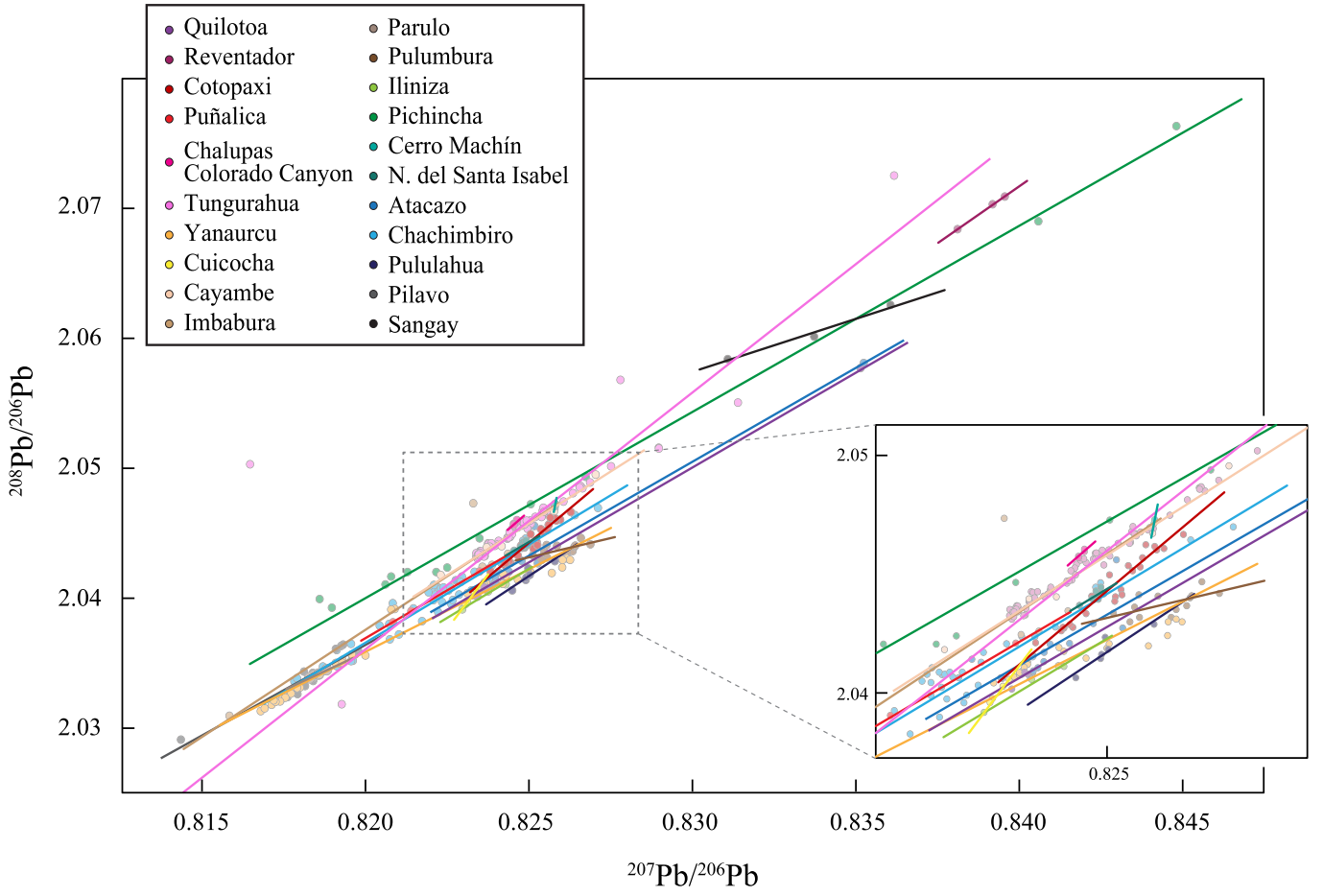

Fig. 5. $^{208}Pb/^{206}Pb$ vs. $^{207}Pb/^{206}Pb$ diagrams at the scale of the Northern Andes, showing the different correlation lines obtained for proximal products from Ecuadorian and Colombian volcanoes (this study; Béguelin et al., 2015; Ancellin et al., 2017; Nauret et al., 2018; Errázuriz-Henao et al., 2019; Bellver-Baca et al., 2020; Chiaradia et al., 2021; the database is given in Appendix F). Because mass fractionation of Pb isotopes is not precisely corrected during conventional measurements by thermal ionization mass spectrometry (TIMS; e.g., White et al., 2000), we only considered analyses performed by MC-ICP-MS, for which mass dependent isotopic fractionation can be corrected using a thallium standard. Equations of regression lines and coefficients of determination (R^2) are given in Table 1. N.: Nevado.

Similarly, Pb isotope ratios of marine tephra ***AMAD-41*** (core KAMAf07; Fig. 1) associated with the Colombian Cerro Machín volcano fit on the correlation line of this latter (turquoise line, Fig. 6e), although it is determined based on only 3 analyses and presents equation parameters that differ significantly from that of other volcanoes (Table 1).

Distal ash ***CAN-2***, sampled in the coastal region and correlated to the last eruption of Quilotoa (Vallejo Vargas, 2011), also plots on the correlation line of this volcano (purple line, Fig. 6f).

Samples ***ATAC-51***, ***-52***, ***-58*** and ***AMAD-37*** and ***-43*** (cores KAT15, 18, 21 and KAMA02; Fig. 1), correlated to the eruptive history of Atacazo-Ninahuilca, are more scattered (Fig. 6d). Without further information like major and trace element contents or age constraints, the identification of the volcanic source of these tephra layers may be biased.

Finally, ***AMAD-40*** (core KAMA19; Fig. 1) belongs to the 10th century eruption of Guagua Pichincha (Bablon et al., 2022), and plots well on the correlation line of Pichincha volcano (green line, Fig. 6b).

Although Pb isotope ratios support the previously established correlations, we note that other sources can be inferred if we consider only these data, due to the proximity of the correlation lines. For example, sample CAN-2 could be correlated with Quilotoa or Iliniza volcanoes (purple and light green lines, Fig. 6a), ATAC-45, -46 and -49 could be associated with Cotopaxi or Chachimbiro volcanoes (red and light blue lines, Fig. 6a), and AMAD-41 could be from Cerro Machín, Pichincha or possibly Tungurahua (turquoise, green and pink lines, Fig. 6a). However, Iliniza and Tungurahua can be discarded because they did not experience such large eruptions during the Holocene, and the age of major eruptions of Chachimbiro and Pichincha volcanoes are inconsistent with the stratigraphic position of ATAC-45, -46, -49 and AMAD-41 tephra layers. Our method therefore allows to narrow down to 2-3 possible volcanic sources, and requires to be combined with other approaches (i.e., geochronology, stratigraphy, geochemistry, knowledge of past major eruptions, spatial distribution of deposits) to reliably identify the source of the distal tephra.

6.3.2. Case of distal tephra whose source needs confirmation

The volcanic source of three distal tephra located in the coastal region needs to be confirmed, as no geochemical or geochronological data are available for these deposits. Results have been plotted with orange stars in Fig. 6.

Three tephra layers have been identified NE of Canoa city (RMC-2 site, Fig. 1a). The uppermost layer has been robustly correlated to the eruption of Quilotoa volcano (RMC-1 in Vallejo Vargas, 2011). Under this layer, ***RMC-2*** pumice bed has a mineral assemblage of Pl and Amp with very scarce Qz and Bt. It has been correlated to the 2335–2600 cal BP eruptive event of Pululahua volcano based on its stratigraphic position and mineral assemblage (Vallejo Vargas, 2011), but its $^{207}Pb/^{206}Pb$ and $^{208}Pb/^{206}Pb$ ratios are closer to those of Quilotoa and Atacazo-Ninahuilca volcanoes (Fig. 6a and d). Products from Quilotoa are characterized by a higher abundance of biotite crystals, we therefore discard this source. The mineral as-

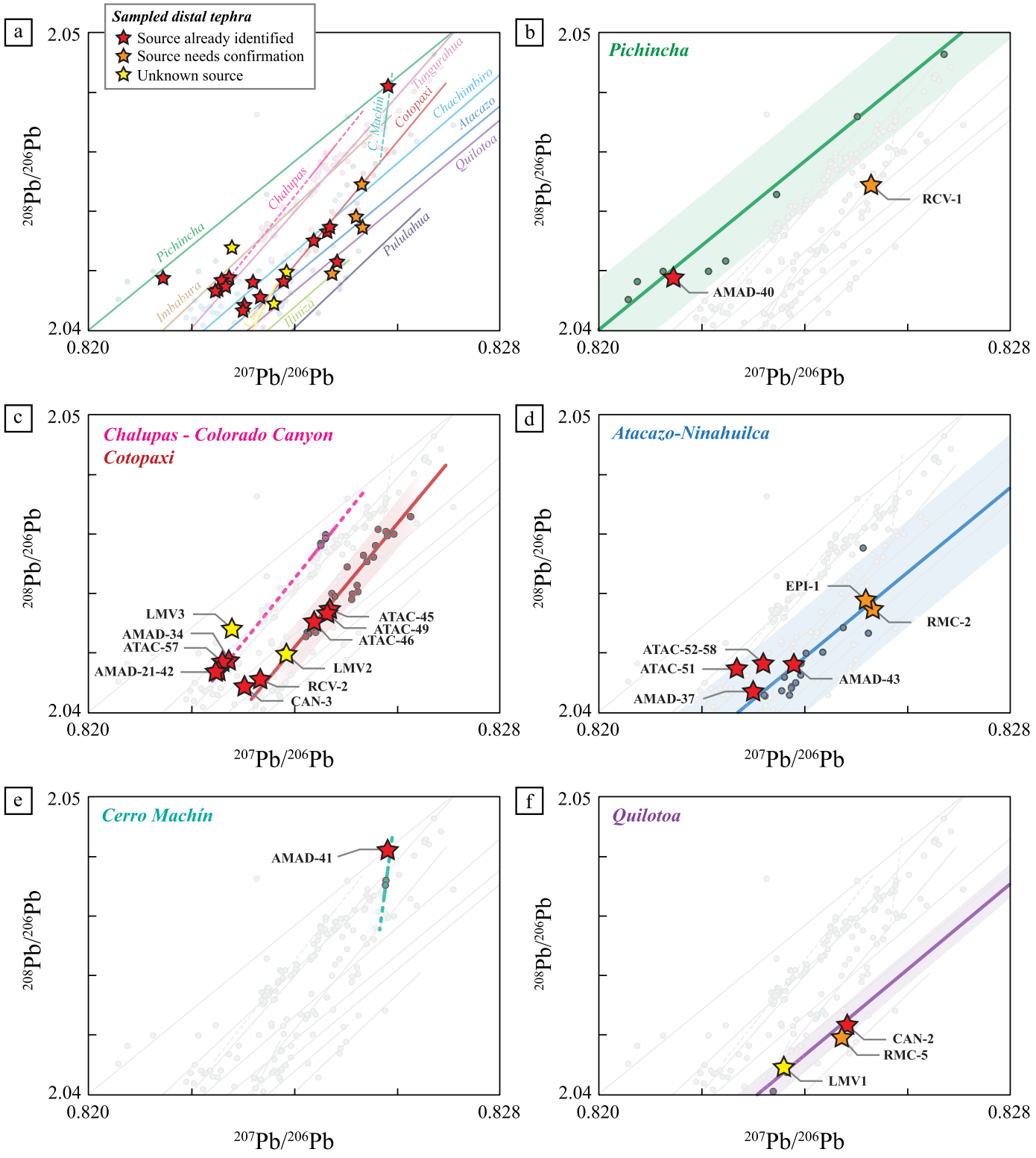

Fig. 6. $^{208}Pb/^{206}Pb$ vs. $^{207}Pb/^{206}Pb$ diagrams showing the ratios obtained for distal tephra compared to regression lines obtained on proximal deposits (same references as Fig. 3). Red star: tephra samples that have been robustly correlated to proximal products (Vallejo Vargas, 2011; Bablon et al., 2022). Orange star: distal tephra samples whose origin is only constrained by their mineralogy and needs to be strengthened. Yellow star: distal sample whose volcanic source is unknown. As all deposits have been emitted during the Holocene based on ^{14}C data, stratigraphy and field evidence, we have discarded Pb data of volcanoes that did not experience a major explosive eruption during this period. Colored areas represent the 95% confidence interval. It is smaller than the point size for Cerro Machín and Chalupas – Colorado Canyon data. Note that the scale is the same for all graphs.

Table 1
Summary of the equations of regression line (Fig. 5), coefficients of determination (R^2), and number of available Pb isotopic analyses for volcanoes from the Northern Andes. *: volcanic centers that experienced major explosive eruptions during the Holocene, whose deposits are key stratigraphic markers in the Northern Andes.

Volcano	Location	Equation of the regression line	R^2	Number of analyses	Age of analyzed samples	Source of Pb data
Atacazo-Ninahuilca*	Ecuador	$y = 1.46x + 0.84$	0.97	17	~1.3 Ma to ~2350 cal BP	This study Ancellin et al. (2017)
Cayambe	Ecuador	$y = 1.60x + 0.73$	0.98	5	~1.1 Ma to Late Holocene	Ancellin et al. (2017)
Chachimbiro*	Ecuador	$y = 1.51x + 0.80$	0.95	47	< 400 ka	Ancellin et al. (2017) Bellver-Baca et al. (2020)
Chalupas – Colorado Canyon*	Ecuador	$y = 2.82x + 0.91$	0.91	4	~216 ka and 4530–5320 cal BP	This study Ancellin et al. (2017)
Cerro Machín*	Colombia	$y = 23.0x - 17.0$	1.00	3	Holocene	Errázuriz-Henao et al. (2019)
Cotopaxi*	Ecuador	$y = 2.07x + 0.33$	0.94	24	Holocene	This study
Cuicocha*	Ecuador	$y = 3.01x + 0.44$	1.00	4	~3000 cal BP	This study Ancellin et al. (2017)
Iliniza	Ecuador	$y = 1.48x + 0.82$	0.98	3	< 350 ka	Ancellin et al. (2017)
Imbabura	Ecuador	$y = 1.65x + 0.68$	0.87	6	Late Pleistocene-Holocene	Ancellin et al. (2017)
Nevado del Santa Isabel*	Colombia	$y = 1.44x + 0.86$	0.63	13	Unknown (Quaternary)	Errázuriz-Henao et al. (2019)
Parulo	Ecuador	$y = 1.18x + 1.07$	0.99	4	< 40 ka	Chiaradia et al. (2021)
Pichincha*	Ecuador	$y = 1.43x + 0.87$	0.99	13	Late Holocene	This study Ancellin et al. (2017)
Pilavo	Ecuador	$y = 1.38x + 0.90$	0.90	14	< 40 ka	Ancellin et al. (2017) Chiaradia et al. (2021)
Pululahua*	Ecuador	$y = 1.65x + 0.68$	0.83	6	Late Pleistocene-Holocene	This study Ancellin et al. (2017)
Pulumbura	Ecuador	$y = 0.57x + 1.57$	0.38	13	12–13 Ma	Chiaradia et al. (2021)
Puñalica	Ecuador	$y = 1.47x + 0.83$	1.00	3	~18 ka	Ancellin et al. (2017)
Quilotoa*	Ecuador	$y = 1.48x + 0.82$	1.00	4	730–680 cal BP	This study Ancellin et al. (2017)
Reventador	Ecuador	$y = 1.75x + 0.60$	1.00	3	Late Holocene	Ancellin et al. (2017)
Sangay	Ecuador	$y = 0.83x + 1.37$	0.98	3	Late Holocene	Ancellin et al. (2017)
Tungurahua*	Ecuador	$y = 1.97x + 0.42$	0.95	85	Holocene	Ancellin et al. (2017) Nauret et al. (2018)
Yanaurcu	Ecuador	$y = 1.26x + 1.00$	0.97	41	< 200 ka	Béguelin et al. (2015)

semblage of RMC-2 is quite consistent with products of the N6 2200–2240 cal BP eruptive event of Atacazo-Ninahuilca, as well as the location of the sampling site with respect to the dispersion axis of products of this eruption (Hidalgo et al., 2008; Vallejo Vargas, 2011). A third tephra layer lying at a depth of 5.3 m has been correlated to the N6 event of Atacazo-Ninahuilca volcano based on its stratigraphic position and mineral assemblage (RMC-4 in Vallejo Vargas, 2011). Considering that it lies under the tephra layer correlated to the N6 event based on our new Pb data, and that tephra layers seem undisturbed, we suggest that it has been emitted during the N5 4880–4940 cal BP event. However, geochemical data of major and trace element contents would be necessary to confirm this stratigraphic sequence.

Six km west of this site, ***RMC-5*** tephra layer (Fig. 1a) is mainly composed of pumices (90%), with a minor amount of free crystals (Pl + Amp + Qz ± Bt; Vallejo Vargas, 2011). It has been correlated to the eruptive history of Cotopaxi (Vallejo Vargas, 2011), although it contains more amphibole crystals than proximal products of this volcano. Our new Pb data suggest that it more likely belongs to the Quilotoa volcano (Fig. 6f), with a composition very close to sample CAN-2, located only 1.6 km south (Fig. 1a).

South of Manta peninsula, ***EPI-1*** (Fig. 1a) is a white tephra layer with a mineral assemblage (Pl + Qz + Amp ± Opx ± Cpx, Vallejo Vargas, 2011) suggesting that it belongs to Pichincha or Atacazo-Ninahuilca volcanoes. Our Pb data suggest that Atacazo-Ninahuilca is the most likely source (Fig. 6d). Tephra from the N4 6170–6310 cal BP event have been identified in marine cores KAT-18, -20, -21 and KAMA-02 (Fig. 1; Bablon et al., 2022), north of the sampling site of EPI-1, but more data are needed to test this hypothesis that sample EPI-1 belongs to this event.

Finally, sample ***RCV-1*** (Fig. 1a) has been correlated to the 3890–3930 cal BP eruptions of Pichincha volcano (Vallejo Vargas, 2011), but does not plot on the correlation line of Pichincha (green line, Fig. 6b). Its Pb ratios are close to those of Cotopaxi and Chachimbiro (red and light blue lines, Fig. 6a). Cotopaxi volcano can be discarded due to the low K_2O content of this sample (1.8 wt.%; i.e. typical of the Western Cordillera; Vallejo Vargas, 2011), and to its lack of biotite crystals, which are abundant in the F rhyolite series of Cotopaxi. In addition, the largest eruption of Chachimbiro was not powerful enough for the tephra to reach the coastal region (Bernard et al., 2014). Pichincha volcano is therefore the most likely source, and the distance of the sample from the correlation line may be explained by the statistical dispersion of the composition of products.

6.3.3. *Case of distal tephra with unknown volcanic source*

The volcanic source of three distal tephra layers, represented with yellow stars in Fig. 6, is not constrained given the absence of geochemical, geochronological, and stratigraphic data.

Sample ***LMV3*** is located in the Eastern Cordillera northeast of the Chalupas caldera (Fig. 1). Mothes and Hall (2008) reported the presence of ash from Quilotoa in that area, but the Pb isotopic composition of LMV3 tephra is significantly different from products of this volcano. Instead, LMV3 has a Pb isotopic composition close to products from the Chalupas caldera and Colorado Canyon event (pink line, Fig. 6c). Chalupas caldera did not experience any large rhyolitic eruption since ~215 ka (Córdova, 2018), and ignimbrite deposits associated with this major eruption are several meters thick and easily recognizable in the cordillera. The remaining possible source of LMV3 distal tephra is therefore the Colorado Canyon event. If this hypothesis is confirmed by the major-trace element analysis of LMV3, this would be the first documented record of tephra dispersal of this eruption in this area.

Sample ***LMV2***, located east of Manta peninsula (Fig. 1a), fits well with the correlation line of Cotopaxi volcano (red line, Fig. 6c). This source is in agreement with the westward transport of tephra from large Holocene eruptions of Cotopaxi by the prevailing winds (Hall and Mothes, 2008b; Vallejo Vargas, 2011; Bablon et al., 2022), but further geochronologic constraints are required to identify to which specific event LMV2 distal tephra belongs.

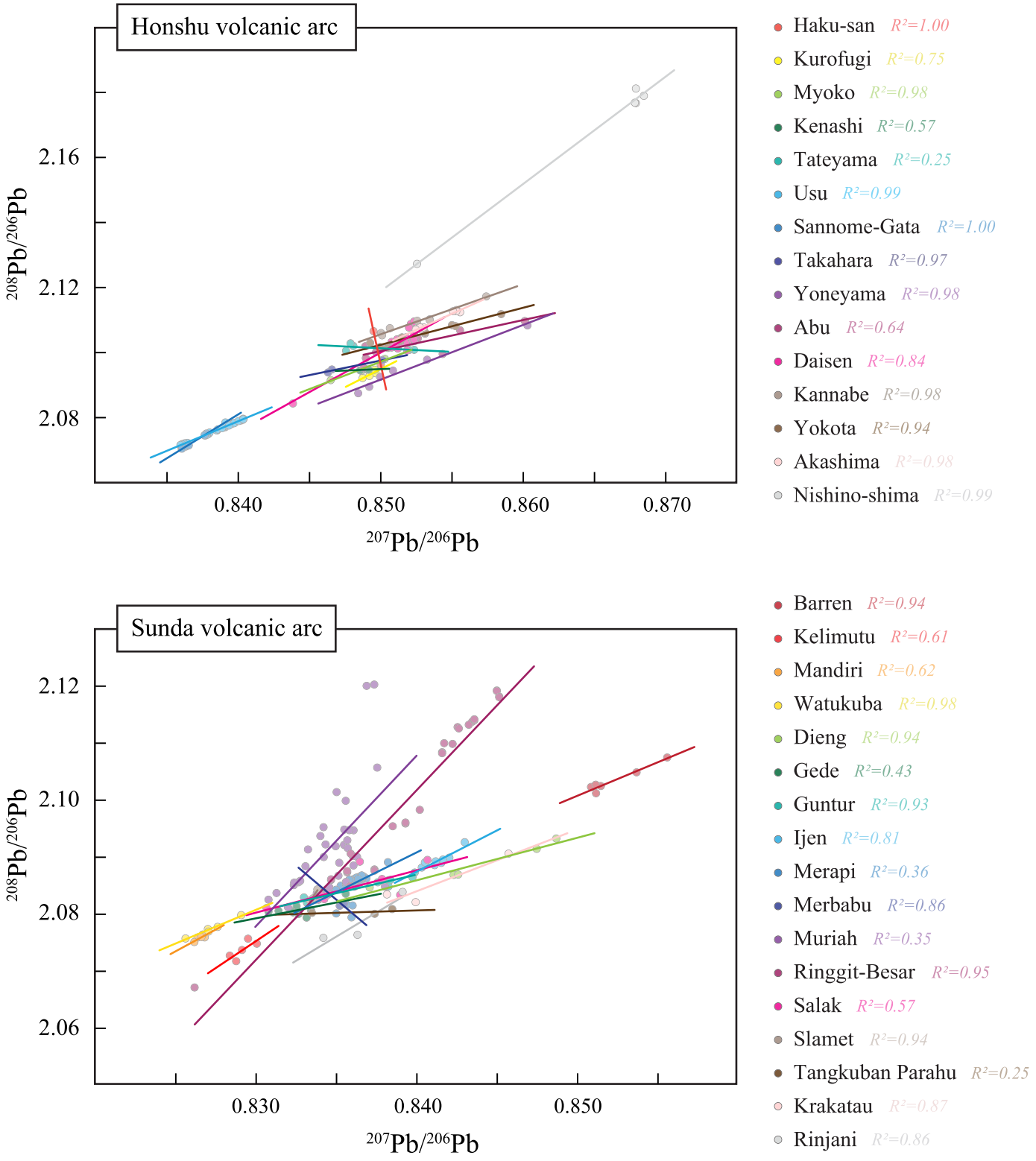

Fig. 7. $^{208}Pb/^{206}Pb$ vs. $^{207}Pb/^{206}Pb$ diagrams showing the regression lines obtained for volcanic complexes, stratovolcanoes, and volcanic islands of Honshu and Sunda arcs (ICP-MS Pb analyzes are from the Georoc database; https://georoc.eu). The typology of volcanic centers from both arcs includes stratovolcanoes (e.g., Hakusan, Usu, Guntur, Merapi), clusters of monogenetic volcanoes and lava domes (e.g., Kannabe, Kurofugi), calderas (e.g., Krakatoa), and volcanic islands (e.g., Nishino-shima, Barren). Plio-Quaternary products belong to the tholeiite and calc-alkaline magmatic series for the Honshu arc, and to the calc-alkaline and shoshonitic series for the Sunda arc (e.g., Turner and Foden, 2001; Kimura and Yoshida, 2006).

Finally, sample ***LMV1***, located at the western foot of the Western Cordillera, ~27 km northwest of Quilotoa caldera (Fig. 1f), has one of the lowest $^{208}Pb/^{206}Pb$ ratios (Fig. 6a). Its Pb composition is close to proximal products of Quilotoa (Fig. 6f), which thus seems to be the most likely source of this sample.

In summary, distal tephra may have an isotopic composition similar to that of a volcano, although the latter is not the source of the tephra (i.e., case of close isotopic signatures, which can be distinguished by alignments in the $^{207}Pb/^{206}Pb$-$^{208}Pb/^{206}Pb$ diagram, for example here for Cotopaxi and Atacazo volcanoes). Conversely, the composition of a distal tephra may not correspond to the isotopic field of their volcanic source (i.e., case of a data point falling on the extension of the $^{207}Pb/^{206}Pb$-$^{208}Pb/^{206}Pb$ alignment of the volcano, for example here for the Colorado Canyon and Cerro Machín events). The combination of $^{207}Pb/^{206}Pb$ and $^{208}Pb/^{206}Pb$ ratios appears to be a strong and suitable tool to decipher the volcanic source of distal tephra, and to narrow down potential sources when geochronological and geochemical data are not available.

6.3.4. First attempt of application of our method to other subduction zones

This study was possible in Ecuador thanks to a large data set of Pb isotope analyses, and to the well-studied major eruptions and associated tephra records. A challenging forthcoming step would be to apply our method to other subduction zones. We made a first attempt with the Honshu and Sunda arcs in Japan and Indonesia, respectively, where more than 200 Pb isotope ratios of past volcanic eruptions have been published (Georoc database). As in Ecuador, $^{207}Pb/^{206}Pb$ *vs.* $^{208}Pb/^{206}Pb$ ratios (Fig. 7) display that equation parameters differ from one volcanic center to another for both arcs, allowing to decipher the source of distal tephra. In addition, Pb isotope ratios are strongly correlated, the average of R^2 being 0.86 and 0.72 for the Honshu and Sunda arcs, respectively. We anticipate that our new isotopic method can be applied to both areas and provide future targets for the development of marine tephrochronology studies. Obviously, we acknowledge that this first attempt is preliminary, and further new Pb measurements of products from Holocene explosive volcanoes will be necessary to validate our new isotopic method for identifying the source of distal tephra.

7. Conclusion

In this study, we use for the first time $^{208}Pb/^{206}Pb$ and $^{207}Pb/^{206}Pb$ ratios on bulk rock to characterize eruptive products from the Northern Andean arc and to identify the volcanic source of distal tephra layers. We first demonstrate that proximal pumices emitted by Cotopaxi volcano (Ecuador) define a straight line in the 2-D $^{208}Pb/^{206}Pb$-$^{207}Pb/^{206}Pb$ space, whose slope and y-intercept depend on the nature/composition of the components involved in the magma genesis processes. We also show that this line does not depend on the age, mineral assemblage, degree of magmatic differentiation, and type of material of the emitted products. Using an extensive database of Pb isotope measurements carried out on proximal lava flows and tephra, we show that each volcano from the Northern Andes can be defined by its own regression line in a $^{208}Pb/^{206}Pb$ *vs.* $^{207}Pb/^{206}Pb$ diagram. We then used this geochemical characteristic to correlate distal tephra layers to volcanic sources. Although the determination of major and trace element contents as well as temporal constraints are necessary to refine the source and age of distal tephra, the combination of $^{207}Pb/^{206}Pb$-$^{208}Pb/^{206}Pb$ ratios is particularly suitable to identify their volcanic source. This method aims to be generalized to all subduction zones where the volcanic activity is explosive and the geodynamic context sufficiently diverse for the magmas to generate significant variations in Pb isotope composition.

CRediT authorship contribution statement

Mathilde Bablon: Conceptualization, Funding acquisition, Investigation, Writing – original draft, Writing – review & editing. **François Nauret:** Conceptualization, Funding acquisition, Investigation, Writing – original draft, Writing – review & editing. **Marianne Saillard:** Conceptualization, Funding acquisition, Investigation, Writing – review & editing. **Pablo Samaniego:** Conceptualization, Investigation, Writing – review & editing. **Ivan Vlastélic:** Investigation, Writing – review & editing. **Silvana Hidalgo:** Investigation. **Jean-Luc Le Pennec:** Investigation, Writing – review & editing. **Gueorgui Ratzov:** Conceptualization, Investigation, Writing – review & editing. **François Michaud:** Conceptualization, Investigation. **Patricia Mothes:** Investigation. **Céline Liorzou:** Investigation. **Abdelmouhcine Gannoun:** Investigation, Writing – review & editing.

Declaration of competing interest

The authors declare that they have no known competing financial interests or personal relationships that could have appeared to influence the work reported in this paper.

Data availability

All data are given in Appendix files.

Acknowledgements

The authors are grateful to Phil Shane, Roberto Sulpizio, and an anonymous reviewer, as well as to Editor Chiara Maria Petrone, for their constructive reviews and useful suggestions, which helped us to improve the final version of this paper. We wish to thank Natasha Sainlot, Daniel Andrade, Silvia Vallejo, Claude Robin, and Michel Monzier (†) for their help during field trips and sampling, and for having entrusted us with some samples of their collections. We also thank Jean-Noël Proust and Jean-Yves Collot for the coring and sampling of marine tephra layers. M. Bablon greatly thanks IODP France for the postdoc fellowship that made this work possible. Geochemical data presented in this paper were funded by the Observatoire de la Côte d'Azur (BQR 2022 grant), and the French Government Laboratory of Excellence initiative n° ANR-10-LABX-0006. This work was also supported by the Tellus Aléas Program of CNRS-INSU (INSU 2019-ALEAS) and is part of the ANR MARACAS program (ANR-18-CE31-0022), and the Laboratoire Mixte International "Séismes et Volcans dans les Andes du Nord" program, an Ecuadorian-French cooperation program between the IG-EPN and the French National Research Institute for Sustainable Development (IRD). This is contribution number 606 of the ClerVolc Program of the International Research Center for Disaster Sciences and Sustainable Development of the University of Clermont Auvergne.

Appendix. Supplementary material

Supplementary material related to this article can be found online at https://doi.org/10.1016/j.epsl.2023.118283.

References

Almeida, M.A., Bablon, M., Andrade, D., Hidalgo, S., Quidelleur, X., Vásconez, F.J., Vásconez Müller, A., Lahitte, P., Samaniego, P., 2023. New geological and geochronological constraints on the evolution of the Cotacachi – Cuicocha Volcanic Complex (Ecuador). J. South Am. Earth Sci., 104489. https://doi.org/10.1016/j.jsames.2023.104489.

Ancellin, M.-A., Samaniego, P., Vlastélic, I., Nauret, F., Gannoun, A., Hidalgo, S., 2017. Across-arc versus along-arc Sr-Nd-Pb isotope variations in the Ecuadorian volcanic arc. Geochem. Geophys. Geosyst. 18, 1163–1188. https://doi.org/10.1002/2016GC006679.

Ancellin, M.-A., Vlastélic, I., Samaniego, P., Nauret, F., Gannoun, A., Hidalgo, S., 2019. Up to 1% Pb isotope disequilibrium between minerals hosted in dacites from the Guagua Pichincha volcano, Ecuador: implication for tracing the source and crustal history of continental arc magmas. Chem. Geol. 525, 177–189. https://doi.org/10.1016/j.chemgeo.2019.07.016.

Andrade, S.D., Müller, A.V., Vasconez, F.J., Beate, B., Aguilar, J., Santamaría, S., 2021. Pululahua dome complex, Ecuador: eruptive history, total magma output and potential hazards. J. South Am. Earth Sci. 106, 103046. https://doi.org/10.1016/j.jsames.2020.103046.

Arculus, R.J., Powell, R., 1986. Source component mixing in the regions of arc magma generation. J. Geophys. Res. 91, 5913. https://doi.org/10.1029/JB091iB06p05913.

Bablon, M., Quidelleur, X., Samaniego, P., Le Pennec, J.-L., Audin, L., Jomard, H., Baize, S., Liorzou, C., Hidalgo, S., Alvarado, A., 2019. Interactions between volcanism and geodynamics in the southern termination of the Ecuadorian arc. Tectonophysics 751, 54–72. https://doi.org/10.1016/j.tecto.2018.12.010.

Bablon, M., Quidelleur, X., Samaniego, P., Le Pennec, J.-L., Santamaría, S., Liorzou, C., Hidalgo, S., Eschbach, B., 2020. Volcanic history reconstruction in northern Ecuador: insights for eruptive and erosion rates on the whole Ecuadorian arc. Bull. Volcanol. 82, 11. https://doi.org/10.1007/s00445-019-1346-1.

Bablon, M., Ratzov, G., Nauret, F., Samaniego, P., Michaud, F., Saillard, M., Proust, J.-N., Le Pennec, J.-L., Collot, J.-Y., Devidal, J., Orange, F., Liorzou, C., Migeon, S., Vallejo, S., Hidalgo, S., Mothes, P., Gonzalez, M., 2022. Holocene marine tephra offshore Ecuador and Southern Colombia: first trench-to-arc correlations and implication for magnitude of major eruptions. Geochem. Geophys. Geosyst. 23. https://doi.org/10.1029/2022GC010466.

Barberi, F., Coltelli, M., Ferrara, G., Innocenti, F., Navarro, J.M., Santacroce, R., 1988. Plio-quaternary volcanism in Ecuador. Geochem. Mag. 125, 1–14.

Béguelin, P., Chiaradia, M., Beate, B., Spikings, R., 2015. The Yanaurcu volcano (Western Cordillera, Ecuador): a field, petrographic, geochemical, isotopic and geochronological study. Lithos 218–219, 37–53. https://doi.org/10.1016/j.lithos.2015.01.014.

Bellver-Baca, M.T., Chiaradia, M., Beate, B., Beguelin, P., Deriaz, B., Mendez-Chazarra, N., Villagómez, D., 2020. Geochemical evolution of the Quaternary Chachimbiro Volcanic Complex (frontal volcanic arc of Ecuador). Lithos 356–357, 105237. https://doi.org/10.1016/j.lithos.2019.105237.

Belshaw, N.S., Freedman, P.A., O'Nions, R.K., Frank, M., Guo, Y., 1998. A new variable dispersion double-focusing plasma mass spectrometer with performance illustrated for Pb isotopes. Int. J. Mass Spectrom. 181, 51–58. https://doi.org/10.1016/S1387-3806(98)14150-7.

Bernard, B., Andrade, D., 2011. Volcanes Cuaternarios del Ecuador Continental. Map 1:500000.

Bernard, J., Kelfoun, K., Le Pennec, J.-L., Vallejo Vargas, S., 2014. Pyroclastic flow erosion and bulking processes: comparing field-based vs. modeling results at Tungurahua volcano, Ecuador. Bull. Volcanol. 76. https://doi.org/10.1007/s00445-014-0858-y.

Bourne, A.J., Lowe, J.J., Trincardi, F., Asioli, A., Blockley, S.P.E., Wulf, S., Matthews, I.P., Piva, A., Vigliotti, L., 2010. Distal tephra record for the last ca 105,000 years from core PRAD 1-2 in the central Adriatic Sea: implications for marine tephrostratigraphy. Quat. Sci. Rev. 29, 3079–3094. https://doi.org/10.1016/j.quascirev.2010.07.021.

Brown, R.J., Bonadonna, C., Durant, A.J., 2012. A review of volcanic ash aggregation. Phys. Chem. Earth Parts A/B/C 45–46, 65–78. https://doi.org/10.1016/j.pce.2011.11.001.

Bryant, J.A., Yogodzinski, G.M., Hall, M.L., Lewicki, J.L., Bailey, D.G., 2006. Geochemical constraints on the origin of volcanic rocks from the Andean northern volcanic zone, Ecuador. J. Petrol. 47, 1147–1175. https://doi.org/10.1093/petrology/egl006.

Carey, S.N., Sigurdsson, H., 1982. Influence of particle aggregation on deposition of distal tephra from the May 18, 1980, eruption of Mount St. Helens volcano. J. Geophys. Res. 87, 7061–7072. https://doi.org/10.1029/JB087iB08p07061.

Caron, B., Siani, G., Sulpizio, R., Zanchetta, G., Paterne, M., Santacroce, R., Tema, E., Zanella, E., 2012. Late Pleistocene to Holocene tephrostratigraphic record from the Northern Ionian Sea. Mar. Geol. 311–314, 41–51. https://doi.org/10.1016/j.margeo.2012.04.001.

Chiaradia, M., Bellver-Baca, M.T., Valverde, V., Spikings, R., 2021. Geochemical and isotopic variations in a frontal arc volcanic cluster (Chachimbiro-Pulumbura-Pilavo-Yanaurcu, Ecuador). Chem. Geol. 574, 120240. https://doi.org/10.1016/j.chemgeo.2021.120240.

Córdova, M., 2018. Identificación y caracterización de los últimos productos eruptivos de la fase resurgente de la caldera de Chalupas. Engineering thesis. Escuela Politécnica Nacional, Quito, Ecuador. 133 pp.

Costa, A., Folch, A., Macedonio, G., Giaccio, B., Isaia, R., Smith, V.C., 2012. Quantifying volcanic ash dispersal and impact of the Campanian Ignimbrite super-eruption. Geophys. Res. Lett. 39. https://doi.org/10.1029/2012GL051605.

Cotten, J., Le Dez, A., Bau, M., Caroff, M., Maury, R.C., Dulski, P., Fourcade, S., Bohn, M., Brousse, R., 1995. Origin of anomalous rare-earth element and yttrium enrichments in subaerially exposed basalts: evidence from French Polynesia. Chem. Geol. 119, 115–138.

D'Antonio, M., Mariconte, R., Arienzo, I., Mazzeo, F.C., Carandente, A., Perugini, D., Petrelli, M., Corselli, C., Orsi, G., Principato, M.S., Civetta, L., 2016. Combined Sr-Nd isotopic and geochemical fingerprinting as a tool for identifying tephra layers: application to deep-sea cores from Eastern Mediterranean Sea. Chem. Geol. 443, 121–136. https://doi.org/10.1016/j.chemgeo.2016.09.022.

Davidson, J., Tepley, F., Palacz, Z., Meffan-Main, S., 2001. Magma recharge, contamination and residence times revealed by in situ laser ablation isotopic analysis of feldspar in volcanic rocks. Earth Planet. Sci. Lett. 184, 427–442. https://doi.org/10.1016/S0012-821X(00)00333-2.

Davidson, J.P., Morgan, D.J., Charlier, B.L.A., Harlou, R., Hora, J.M., 2007. Microsampling and isotopic analysis of igneous rocks: implications for the study of magmatic systems. Annu. Rev. Earth Planet. Sci. 35, 273–311. https://doi.org/10.1146/annurev.earth.35.031306.140211.

DePaolo, D.J., 1981. Trace element and isotopic effects of combined wallrock assimilation and fractional crystallization. Earth Planet. Sci. Lett. 53, 189–202. https://doi.org/10.1016/0012-821X(81)90153-9.

Di Muro, A., Rosi, M., Aguilera, E., Barbieri, R., Massa, G., Mundula, F., Pieri, F., 2008. Transport and sedimentation dynamics of transitional explosive eruption columns: the example of the 800 BP Quilotoa plinian eruption (Ecuador). J. Volcanol. Geotherm. Res. 174, 307–324. https://doi.org/10.1016/j.jvolgeores.2008.03.002.

Errázuriz-Henao, C., Gómez-Tuena, A., Duque-Trujillo, J., Weber, M., 2019. The role of subducted sediments in the formation of intermediate mantle-derived magmas from the Northern Colombian Andes. Lithos 336–337, 151–168. https://doi.org/10.1016/j.lithos.2019.04.007.

Galer, S.J.G., Abouchami, W., 1998. Practical application of lead triple spiking for correction of instrumental mass discrimination. Mineral. Mag. 62A (1), 491–492. https://doi.org/10.1180/minmag.1998.62a.1.260.

Garrison, J.M., Davidson, J.P., Hall, M., Mothes, P., 2011. Geochemistry and petrology of the most recent deposit from Cotopaxi Volcano, Northern Volcanic Zone, Ecuador. J. Petrol. 52, 1641–1678. https://doi.org/10.1093/petrology/egr023.

Guillaume-Gentil, N., 2008. Cinq mille ans d'histoire au pied des volcans en Équateur: modes d'implantation, peuplement et chronologie. Terra Archaeologica VI.

Hall, M., Mothes, P., 2008a. Volcanic impediments in the progressive development of pre-Columbian civilizations in the Ecuadorian Andes. J. Volcanol. Geotherm. Res. 176 (3), 344–355. https://doi.org/10.1016/j.jvolgeores.2008.01.039.

Hall, M., Mothes, P., 2008b. The rhyolitic–andesitic eruptive history of Cotopaxi volcano, Ecuador. Bull. Volcanol. 70, 675–702. https://doi.org/10.1007/s00445-007-0161-2.

Hall, M.L., Mothes, P.A., 1994. Tefroestratigrafía holocénica de los volcanes principales del valle interandino, Ecuador. In: Marocco, R. (Ed.), El Contexto Geológico del Espacio Físico Ecuatoriano. Corporación Editora Nacional, Quito, pp. 47–67.

Hall, M.L., Robin, C., Beate, B., Mothes, P., Monzier, M., 1999. Tungurahua Volcano, Ecuador: structure, eruptive history and hazards. J. Volcanol. Geotherm. Res. 91, 1–21.

Hall, M.L., Samaniego, P., Le Pennec, J.L., Johnson, J.B., 2008. Ecuadorian Andes volcanism: a review of Late Pliocene to present activity. J. Volcanol. Geotherm. Res. 176, 1–6. https://doi.org/10.1016/j.jvolgeores.2008.06.012.

Hanano, D., Scoates, J.S., Weis, D., 2009. Alteration mineralogy and the effect of acid-leaching on the Pb-isotope systematics of ocean-island basalts. Am. Mineral. 94, 17–26. https://doi.org/10.2138/am.2009.2845.

Hidalgo, S., 2006. Les intéractions entre magmas calco-alcalins "classiques" et adakitiques: exemple du complexe volcanique Atacazo-Ninahuilca (Équateur). PhD thesis. Université Blaise Pascal-Clermont-Ferrand II, France.

Hidalgo, S., Gerbe, M.C., Martin, H., Samaniego, P., Bourdon, E., 2012. Role of crustal and slab components in the Northern Volcanic Zone of the Andes (Ecuador) constrained by Sr–Nd–O isotopes. Lithos 132–133, 180–192. https://doi.org/10.1016/j.lithos.2011.11.019.

Hidalgo, S., Monzier, M., Almeida, E., Chazot, G., Eissen, J.-P., van der Plicht, J., Hall, M.L., 2008. Late Pleistocene and Holocene activity of the Atacazo–Ninahuilca Volcanic Complex (Ecuador). J. Volcanol. Geotherm. Res. 176, 16–26. https://doi.org/10.1016/j.jvolgeores.2008.05.017.

Ishikawa, T., Nakamura, E., 1994. Origin of the slab component in arc lavas from across-arc variation of B and Pb isotopes. Nature 370, 205–208. https://doi.org/10.1038/370205a0.

Jackson, L.J., Horton, B.K., Beate, B.O., Bright, J., Breecker, D.O., 2019. Testing stable isotope paleoaltimetry with Quaternary volcanic glasses from the Ecuadorian Andes. Geology. https://doi.org/10.1130/G45861.1.

Jochum, K.P., Nohl, U., Herwig, K., Lammel, E., Stolland, B., Hofmann, A.W., 2005. GeoReM: a new geochemical database for reference materials and isotopic standards. Geostand. Geoanal. Res. 29 (3), 333–338. https://doi.org/10.1111/j.1751-908x.2005.tb00904.x.

Kimura, J.-I., Yoshida, T., 2006. Contributions of slab fluid, mantle wedge and crust to the origin of Quaternary lavas in the NE Japan arc. J. Petrol. 47, 2185–2232. https://doi.org/10.1093/petrology/egl041.

Le Pennec, J.-L., Ramón, P., Robin, C., Almeida, E., 2016. Combining historical and ^{14}C data to assess pyroclastic density current hazards in Baños city near Tungurahua volcano (Ecuador). Quat. Int. 394, 98–114. https://doi.org/10.1016/j.quaint.2015.06.052.

Lowe, D.J., 2011. Tephrochronology and its application: a review. Quat. Geochronol. 6, 107–153. https://doi.org/10.1016/j.quageo.2010.08.003.

Mamani, M., Tassara, A., Wörner, G., 2008. Composition and structural control of crustal domains in the central Andes. Geochem. Geophys. Geosyst. 9, Q03006. https://doi.org/10.1029/2007GC001925.

Mothes, P.A., Hall, M.L., 2008. The plinian fallout associated with Quilotoa's 800 yr BP eruption, Ecuadorian Andes. J. Volcanol. Geotherm. Res. 176, 56–69. https://doi.org/10.1016/j.jvolgeores.2008.05.018.

Nauret, F., Samaniego, P., Ancellin, M.-A., Tournigand, P.-Y., Le Pennec, J.-L., Vlastelic, I., Gannoun, A., Hidalgo, S., Schiano, P., 2018. The genetic relationship between andesites and dacites at Tungurahua volcano, Ecuador. J. Volcanol. Geotherm. Res. 349, 283–297. https://doi.org/10.1016/j.jvolgeores.2017.11.012.

Newnham, R.M., Lowe, D.J., Matthews, B.W., 1998. A late-Holocene and prehistoric record of environmental change from Lake Waikaremoana, New Zealand. Holocene 8, 443–454. https://doi.org/10.1191/095968398672490834.

Nobre Silva, I.G., Weis, D., Barling, J., Scoates, J.S., 2009. Leaching systematics and matrix elimination for the determination of high-precision Pb isotope compositions of ocean island basalts. Geochem. Geophys. Geosyst. 10. https://doi.org/10.1029/2009GC002537.

Nomade, S., Bassinot, F., Marino, M., Simon, Q., Dewilde, F., Maiorano, P., Isguder, G., Blamart, D., Girone, A., Scao, V., Pereira, A., Toti, F., Bertini, A., Combourieu-Nebout, N., Peral, M., Bourlès, D.L., Petrosino, P., Gallicchio, S., Ciaranfi, N., 2019. High-resolution foraminifer stable isotope record of MIS 19 at Montalbano Jonico, southern Italy: a window into Mediterranean climatic variability during a low-eccentricity interglacial. Quat. Sci. Rev. 205, 106–125. https://doi.org/10.1016/j.quascirev.2018.12.008.

Opdyke, N.D., Hall, M., Mejia, V., Huang, K., Foster, D.A., 2006. Time-averaged field at the equator: results from Ecuador. Geochem. Geophys. Geosyst. 7. https://doi.org/10.1029/2005GC001221.

Papale, P., Rosi, M., 1993. A case of no-wind plinian fallout at Pululagua caldera (Ecuador): implications for models of clast dispersal. Bull. Volcanol. 55, 523–535. https://doi.org/10.1007/BF00304594.

Pin, C., Gannoun, A., Dupont, A., 2014. Rapid, simultaneous separation of Sr, Pb, and Nd by extraction chromatography prior to isotope ratios determination by TIMS and MC-ICP-MS. J. Anal. At. Spectrom. 29, 1858–1870. https://doi.org/10.1039/C4JA00169A.

Rehkämper, M., Halliday, A.N., 1998. Accuracy and long-term reproducibility of lead isotopic measurements by multiple-collector inductively coupled plasma mass spectrometry using an external method for correction of mass discrimination. Int. J. Mass Spectrom. 181, 123–133. https://doi.org/10.1016/S1387-3806(98)14170-2.

Robin, C., Samaniego, P., Le Pennec, J.-L., Fornari, M., Mothes, P., van der Plicht, J., 2010. New radiometric and petrological constraints on the evolution of the Pichincha volcanic complex (Ecuador). Bull. Volcanol. 72, 1109–1129. https://doi.org/10.1007/s00445-010-0389-0.

Robin, C., Samaniego, P., Le Pennec, J.-L., Mothes, P., van der Plicht, J., 2008. Late Holocene phases of dome growth and Plinian activity at Guagua Pichincha volcano (Ecuador). J. Volcanol. Geotherm. Res. 176, 7–15. https://doi.org/10.1016/j.jvolgeores.2007.10.008.

Rosi, M., Landi, P., Polacci, M., Di Muro, A., Zandomeneghi, D., 2004. Role of conduit shear on ascent of the crystal-rich magma feeding the 800-year-b.p. Plinian eruption of Quilotoa Volcano (Ecuador). Bull. Volcanol. 66, 307–321. https://doi.org/10.1007/s00445-003-0312-z.

Samaniego, P., Robin, C., Chazot, G., Bourdon, E., Cotten, J., 2010. Evolving metasomatic agent in the Northern Andean subduction zone, deduced from magma composition of the long-lived Pichincha volcanic complex (Ecuador). Contrib. Mineral. Petrol. 160, 239–260. https://doi.org/10.1007/s00410-009-0475-5.

Sarna-Wojcicki, A.M., Davis, J.O., 1991. Chapter 5: Quaternary tephrochronology. In: Quaternary Nonglacial Geology; Conterminous United States. The Geological Society of America, The Geology of North America, Boulder, Colorado.

Schindlbeck, J.C., Kutterolf, S., Freundt, A., Alvarado, G.E., Wang, K.-L., Straub, S.M., Hemming, S.R., Frische, M., Woodhead, J.D., 2016. Late Cenozoic tephrostratigraphy offshore the southern Central American Volcanic Arc: 1. Tephra ages and provenance. Geochem. Geophys. Geosyst. 17, 4641–4668. https://doi.org/10.1002/2016GC006503.

Schindlbeck, J.C., Kutterolf, S., Freundt, A., Straub, S.M., Wang, K.-L., Jegen, M., Hemming, S.R., Baxter, A.T., Sandoval, M.I., 2015. The Miocene Galápagos ash layer record of Integrated Ocean Drilling Program Legs 334 and 344: ocean-island explosive volcanism during plume-ridge interaction. Geology 43, 599–602. https://doi.org/10.1130/G36645.1.

Siani, G., Michel, E., De Pol-Holz, R., DeVries, T., Lamy, F., Carel, M., Isguder, G., Dewilde, F., Lourantou, A., 2013. Carbon isotope records reveal precise timing of enhanced Southern Ocean upwelling during the last deglaciation. Nat. Commun. 4, 2758. https://doi.org/10.1038/ncomms3758.

Timms, R.G.O., Matthews, I.P., Palmer, A.P., Candy, I., 2018. Toward a tephrostratigraphic framework for the British Isles: a Last Glacial to Interglacial Transition (LGIT c. 16-8 ka) case study from Crudale Meadow, Orkney. Quat. Geochronol. 46, 28–44. https://doi.org/10.1016/j.quageo.2018.03.008.

Turner, S., Foden, J., 2001. U, Th and Ra disequilibria, Sr, Nd and Pb isotope and trace element variations in Sunda arc lavas: predominance of a subducted sediment component. Contrib. Mineral. Petrol. 142, 43–57. https://doi.org/10.1007/s004100100271.

Ukstins Peate, I., Baker, J.A., Kent, A.J.R., Al-Kadasi, M., Al-Subbary, A., Ayalew, D., Menzies, M., 2003. Correlation of Indian Ocean tephra to individual Oligocene silicic eruptions from Afro-Arabian flood volcanism. Earth Planet. Sci. Lett. 211, 311–327. https://doi.org/10.1016/S0012-821X(03)00192-4.

Vallejo Vargas, S., 2011. Distribución de las cenizas volcánicas holocénicas – tardías en la Costa del Ecuador. Engineering thesis. Escuela Politécnica Nacional, Quito, Ecuador.

Westgate, J.A., Pearce, N.J.G., Perkins, W.T., Shane, P.A., Preece, S.J., 2011. Lead isotope ratios of volcanic glass by laser ablation inductively-coupled plasma mass spectrometry: application to Miocene tephra beds in Montana, USA and adjacent areas. Quat. Int. 246, 82–96. https://doi.org/10.1016/j.quaint.2011.08.003.

White, W.M., Albarède, F., Télouk, P., 2000. High-precision analysis of Pb isotope ratios by multi-collector ICP-MS. Chem. Geol. 167, 257–270. https://doi.org/10.1016/S0009-2541(99)00182-5.

Wulf, S., Hardiman, M.J., Staff, R.A., Koutsodendris, A., Appelt, O., Blockley, S.P.E., Lowe, J.J., Manning, C.J., Ottolini, L., Schmitt, A.K., Smith, V.C., Tomlinson, E.L., Vakhrameeva, P., Knipping, M., Kotthoff, U., Milner, A.M., Müller, U.C., Christanis, K., Kalaitzidis, S., Tzedakis, P.C., Schmiedl, G., Pross, J., 2018. The marine isotope stage 1–5 cryptotephra record of Tenaghi Philippon, Greece: towards a detailed tephrostratigraphic framework for the Eastern Mediterranean region. Quat. Sci. Rev. 186, 236–262. https://doi.org/10.1016/j.quascirev.2018.03.011.